A thermogravimetric- and X-ray scattering- study of hydration transitions in a nano-layered silicate synthetic clay

Etude par thermogravimétrie et diffusion des rayons X des transitions d'hydratation dans une argile synthétique nano-lamellaire.

Study carried out by :

Simon Dagois-Bohy

delivered on

1st September 2005

under supervision of :

Jon Otto Fossum [1] Ahmed Gmira [2] Yves Méheust[3]

This work has been carried out at the Department of Physics at the Faculty of Natural Sciences and Technology.

[1] Professor, e-mail : jon.fossum@phys.ntnu.no

[2] Post-Doc, e-mail : ahmed.gmira@phys.ntnu.no

[3] Chercheur associé, e-mail : yves.meheust@phys.ntnu.no

Summary

This work is an experimental study of a synthetic layered silicate system. The material under study is fluorohectorite $Li(Mg_2Li)Si_4O_{10}F_2$. Two experimental techniques have been used in order to investigate its microscopic and thermodynamic properties, and sometimes to relate them together, under variable temperature and humidity in a range of 0°C to 140°C and 0% to 95% respectively. Thermogravimetric analysis shows successive absorption of water, depending on the inter-lamellar cation used, and X-ray spectra's out of plane peaks give precise interlayer distances at a given hydration sates. Still, in-plane peaks show that crystallographic unit cell basic vectors do not change during transition. Finally, comparisons between these two types of data shows that for multivalent interlayer cations, a 2-phase transition of the first-order model is not sufficient.

Résumé

Ce travail est une étude expérimentale d'une argile synthétique lamellaire, qui a porté sur la Fluorohectorite $Li(Mg_2Li)Si_4O_{10}F_2$. Deux techniques expérimentales ont été utilisées pour sonder les propriétés microscopiques et thermodynamiques de ce matériau, et parfois les relier entre elles, sous un environnement contrôlé en température et humidité. Les analyse thermogravimétriques mettent en évidence des absorptions successives d'eau, dans des quantités dépendant du cation inter-lamellaire, et les pics hors-plan des spectres aux rayons X donnent précisément les distances inter-lamellaires pour une hydratation donnée. Toutefois, les pics planaires n'indiquent aucune modification significative de la cellule de base dans le plan des lamelles. Enfin, une comparaison entre ces deux types de données montre que pour des cations multivalents, un modèle comprennant deux transitions de phases du premier ordre ne décrit pas bien les résultats obtenus.

Acknowledgments

A lot of people have helped me during this work, and I would like to thank them all.

First of all, Jon Otto Fossum, my main supervisor, without whom nothing of this work could have been possible.

Yves Méheust, also my main supervisor, who helped me a lot on x-ray experiments as well as on the understanding of physical problems involved in clay systems, giving me clear answers nearly every time I needed them.

Ahmed Gmira, who helped me also a lot on TGA experiments as well as in the lab's everyday life.

Kenneth Knudsen, who gave a very kind and valuable help during synchrotron experiments.

Davi Miranda da Fonseca and Kanak Parmar, who helped me a lot in understanding the lab's organisation and finding the coffee machine.

I would like to thank also all the other people from the lab (Marie-céline, Kate, Nils...), as well as the "Moholt group" (they will recognise themselves...) without who life in Trondheim would have been very different...

Contents

Introduction

In early times of geology, clays were defined as the smallest natural mineral structure, with a characteristic size lower than 2μm. But since it has been discovered that a lot of materials with very different properties are included in this definition. Nowadays, clays' definition specify a common structure that has to be shared : clays in natural settings have a phyllosilicate (or silicate leaf) structure. Clay minerals represent a very large family of materials, and there are a lot of subdivision according to greater similarities in particle structures. One of the most important property of some clay minerals is the **swelling property**, i.e. the ability to change volume with the absorption of liquids (mostly water) into their structures. These swelling clays are called smectite, and the present study will focus on a particular type of smectite : the fluorohectorite. The properties of this type of smectite clay have been investigated using mainly two experimental techniques, X-ray Scattering and Thermogravimetry. After a description of fluorohectorite structure and some principles needed for the experimental techniques used, we will describe the experiments and then discuss them.

1 Fluorohectorite, a synthetic swelling clay

1.1 Chemical structure of Smectite clays

fluorohectorite is derived from Hectorite, a Trioctahedral smectite. The basic building block of a smectite clay mineral is a platelet consisting of a so-called hexagonal sheet sandwiched between two so-called tetrahedral sheets [11] (fig 1).

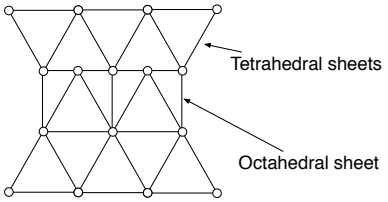

Figure 1:
Here is a side view of the fluorohectorite. Triangles on top and on bottom are part of the SiO4 tetrahedrae, while squares in the middle are octahedrae

The tetrahedral sheet consists of tetrahedrons in which one silicium atom is surrounded by four oxygen anions.

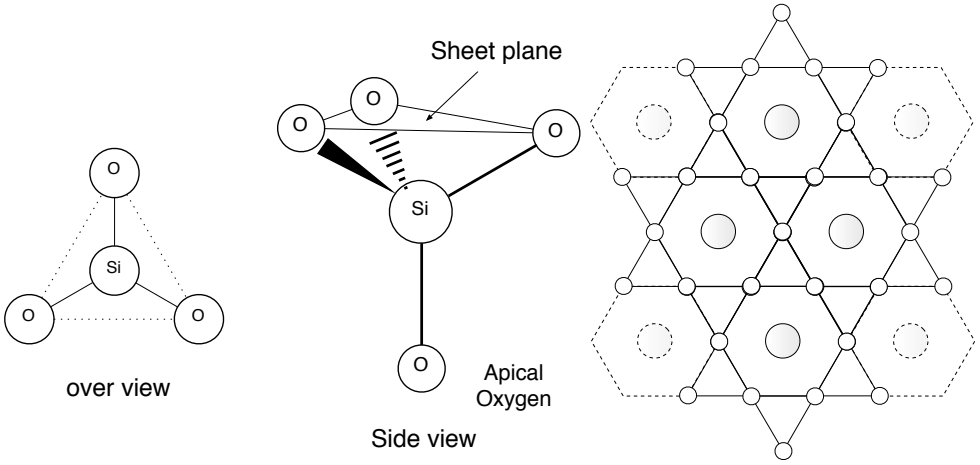

Figure 2: on the left, we can see a tetrahedron from the side and from the top ; on the right we can see how these tetrahedrons form a plane sheet pattern with oxygens (white circles) and Hydroxyls (shaded circles)

Three of these oxygens define the sheet plane, and can be shared between 2 silicium atoms, while the last oxygen of the tetrahedron is called "apical" oxygen and is shared with the octahedron sheet as it will be discussed a bit further. The sheet plane triangles pave this plane with a combination of hexagons and triangles (see fig 2)
The second tetrahedral sheet is almost symmetric to the first one with respect to the equatorial plane of the platelet, but slightly shifted in order to build what will be the octahedral layer in between, linked to the tetrahedral sheets by the apical oxygens.
In usual hectorite, two apical oxygens of two tetrahedral cells from each of the tetrahedral layers, together with two additional hydroxyl groups, create an octahedral cell in which comes a cation (usually Al^{2+}, Mg^{2+} or Fe^{2+}, but also Ti, Ni, Zn, Cr, Mn^{2+}...). The octahedral layer consists of these adjacents octahedral cells.
The resulting basic unit, or platelet, is shown in fig.It is flat on its top and bottom surface,

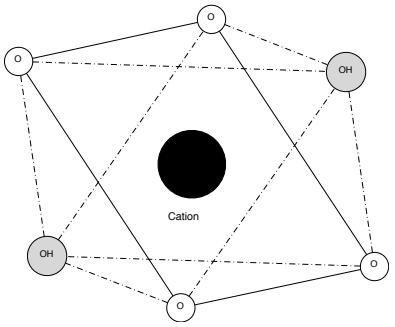

Figure 3: here is an octahedron unit cell : the cation is surrounded by four oxygen and two OH (or F) groups. warning : the lines do not represent any bond between atoms

and 1nm thick. In the following text, we shall call this resulting particle with several equivalent names, like "sheet, platelet" or "particle". Due to the fact that all species at the side of the sheet are oxygen anions, and that sometimes the Si tetrahedrally coordinated cation can be replaced with a less-charged cation (Fe, Al^{3+},...), the planar surfaces are negatively charged, while the edges are slightly positively charged. In the present study we have worked with fluorohectorite, a synthetic hectorite where hydroxyl groups have been replaced by fluorin anions : the result is that fluorohectorite has a surface charge density particularly large for a smectite (1.2 e- per half elementary cell).

1.2 Deck of card - structure of fluorohectorite particle

Interactions between clay platelets in saline solution fluorohectorite charged platelets surely interact one with each other when put in solution. The main forces to be retained are of course Van der Waals attraction, and Electrostatic repulsion. The electrostatic repulsion depends strongly of the ionic power of the solution : in a pure de-ionized water, the screening length (i.e. the characteristic distance after which the electrostatic force resulting from a charged object is cancelled by opposite charged ions in the solution) is very high, and so is the electrostatic force range and intensity : the platelets stay as far from each other than they can. On the contrary, when the solution is highly ionised, the same screen length is very low and Van der Waals can control the platelets positions and make them come closer. However, at a moment, another process appears.

Stacking the platelets In the case of fluorohectorite, some cations in solution may come and fit the hexagonals "holes" (explained before in the structure chapter), just in front of a Fluor, and if the platelets are close enough, these cations can be shared with the opposite platelet.

This is of course not limited to only 2 sheets and therefore a lot of these sheets are able to stack on one to another : the fluorohectorite particles in suspensions have been obverved to consist of up to 100 clay platelets [7], and those deck-of-card like, cation-pillared, fluorohectorite particles are found in "dry" (i.e, weakly-hydrated) samples as well[4]. The characteristic distance between 2 adjacent platelets is called d-spacing, and is the most visible periodicity of these solids.

[4] It is possible to exchange cations if we manage to reduce the electrostatic forces between sheets, (by extreme dilution for instance) and then to replace the type of ions in solution.

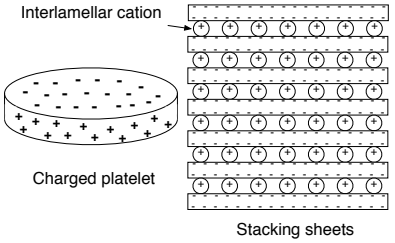

Figure 4: here is a schema of how the platelets can stack one to another and form large cation-pillared particles.

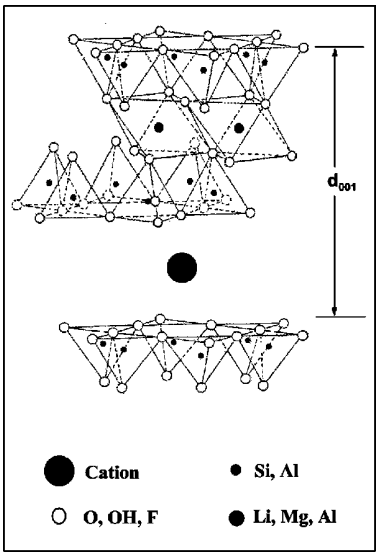

Figure 5: A hectorite full unit cell.
Two platelets can stack together by sharing cations, creating a periodicity in the vertical dimension.

Particle swelling during hydration : one of the most specific properties of cation-pillared-layered smectite clays is the swelling property. In presence of water, a deck-of card particle may absorb some water molecules and increase its height. Though quite intuitive, this phenomenon is not totally understood. There are a few things that are generally accepted [11]

- the layer charge allow only few water "layers" between sheets surfaces
- water forms a coordination sphere (or shell) around interlayer cations
- these water molecules are dynamic, i.e. rotating, vibrating and stretching, in a confined liquid state, between bulk liquid and ice.

The swelling process depends essentially of external thermodynamic parameters such as water pressure and temperature : obviously, the higher the water pressure, the more water is absorbed whereas the higher the temperature, the more water is ejected from interlayer places.

This project consisted essentially in the study of the swelling process under controlled temperature and humidity, study with thermogravimetry and X-rays diffraction.

2 Theory for experimental techniques

2.1 Thermodynamic aspect of the transition, TGA/SDTA

2.1.1 Thermo-Gravimetric analysis

Thermogravimetry consist simply in recording weight of a sample while controlling temperature and atmosphere around it. There are mainly two ways of using a TGA, both with advantages and inconvenients : with constant temperature steps and with constant rate temperature. The constant rate temperature gives more informations, requires less experiments, and incidentally is more easy to perform on the machine used. This method allows, for instance, to see immediately the transition temperatures; it allows also to draw derivative curves $\frac{dm}{dT}$ [3] (see appendix). However there happened to be two major problems using it :

- Whatever small the sample was, there always was bad kinetic, i.e. the sample was always heated too fast, and then all the temperatures quoted were slightly (or not) shifted up (down in case of cooling)
- We discovered that the balance does not functions the same for temperature rates and isothermal steps : the weight measured with no sample present was not 0g when there was temperature variations !

The resulting decision was to record only isothermal steps that could only give valuable information on the equilibrium mass at a given temperature.

2.1.2 Temperatures of transition

In the TGA data, we define the transition temperature as the average of temperatures during which there are a rapid gain or loss of weight. According to the fact that the interlayer water is supposed to be in a state between bulk liquid and ice, and also that we use atmospheric pressure, these temperatures should be higher than the ice-liquid transition temperature, i.e. 0°C.

2.1.3 Gibbs free energy of transition

According to Suzuki et al.[14], we can consider that hydration transitions are first-order transitions, and we can write the gibbs free energy of our smectite sample as : $G = \min_i [G\{i\}]$ where i represents the hydration state and $G\{i\}$ can be expressed as :

$$G\{i\} = [V_i(i) - h]\, n_i + n_c V_e(i)$$

with

$h = RT \ln \frac{P}{P_s(T)}$ is an external field composed with T, P and Ps(T), the saturated water pressure. It can be noted that the expression inside the log is exactly the definition for relative humidity : $RH = P/P_s(T)$.

n_i is the amount of water absorbed. The i index will be explained later

$n_i V_i$ represents the hydration energy per water molecule of the water layer(s)

$Ve(i)$ represents the electrostatic interactions between a cation and the silicate plane, and n_c should be the number of cations.

Looking at the TGA curves, we can see that in first approximation, the amount n of water asorbed evolves almost by steps of constant amounts corresponding to water layers : this is the meaning of the n_i notation : in first approximation, the amount n of water absorbed depends only of the number of water layers. Consequently, each $G\{i\}(h)$ will be a straight line which negative slope will decrease with i, as shown in fig 6. The values

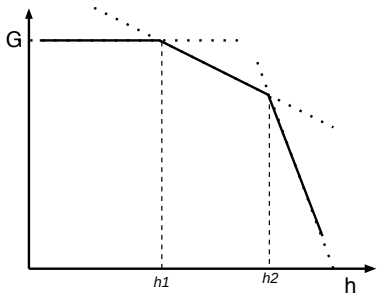

Figure 6: G is approximated as straight lines which steep only depends of the amount of water absorbed, supposed constant for a given hydration state

of h_1 and h_2 can be expressed in function of n, n_c V_e and V by resolving the equations $G\{0\}(h_1) = G\{1\}(h_1)$ and $G\{1\}(h_2) = G\{2\}(h_2)$, which gives :

$$h_1 = V(1) + \frac{n_c}{n_1}\left[Ve(1) - Ve(0)\right]$$

$$h_2 = \frac{1}{n_2 - n_1}\left[n_2 V(2) - n_1 V(1)\right] + \frac{n_c}{n_2 - n_1}\left[V_e(2) - V_e(1)\right]$$

Always according to Suzuki et al [14] , we can assume that the hydration energy is quite the same for both 0-1 and 1-2 transitions, then the condition $h1 < h2$ can be simply expressed in

$$(\frac{n_2}{n_1} - 1)n_c V_e(0) + \frac{n_2}{n_1} n_c V_e(1) - n_c V_e(2) < 0$$

which gives

$$\frac{n_2}{n_1} > \frac{V_e(0) - V_e(2)}{V_e(0) - V_e(1)}$$

and, if we evaluate $V_e(i)$ as an electrostatic potential between a charge and a charged plan : $V_e = -Cst\frac{\sigma^2 Sx}{\epsilon}$ (σ : charge density, S : surface, ϵ : dielectric constant, x cation-platelet distance), we finally have :

$$\frac{n_2}{n_1} > \frac{d(2) - d(0)}{d(1) - d(0)} \tag{1}$$

where d(i) is the interlayer distance for the hydration state i.

2.2 X-rays

2.2.1 Origins and production of X-rays

Origins X-rays were discovered by W.C. Röntgen in nov. 1895 in Wurtzburg, but it is not before 1912, when Von Laue obtained a clear diffraction pattern from a crystal lattice, that it was proved (thanks to the young Bragg) that X-rays are nothing else than **an electromagnetic radiation with a very short wavelength** ($\lambda \simeq 1$Å). Early sources of X-rays used electrons accelerated towards a cooled anode : the impact of the electrons on the anode produces X-ray light. The spectrum of these X-rays has a particular

shape, composed of a large broadened basis due to electrons being decelerated, and several single sharp peaks related to the collision between some accelerated electrons and atomic electrons from the anode : the atomic electron may be removed from an inner shell of an atom, and replaced by another from the outer shell, a relaxation that produces an X-ray with a characteristic energy equal to the difference energy between the two shells.

Synchrotron light Nowadays a very more powerful way of producing X-rays can be used : the Synchotron radiation. This radiation is caused by charged particles (mostly

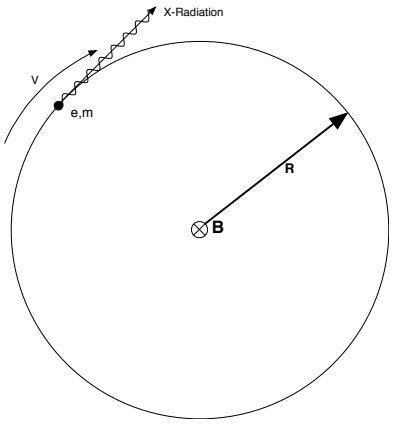

Figure 7: electron orbit in synchrotronradiation

electrons or positrons) rotating at a relativistic speed in a circular trajectory fixed by high magnetic fields. It is known that accelerated charged particles radiates, and a relativistic calculus shows that the characteristic frequency of a pulse is $\omega_c = \gamma^3\omega_0$, where ω_0 is the cycle frequency ($\Omega_0 = v/R$), and $\gamma = 1/\sqrt{1-(\frac{v}{c})^2}$ is the Lorentz factor. For a classical movment, the centripetal acceleration is of the same order of magnitude of the lorenz magnetic force divided by the electron mass : $mv^2/R = evB$ (letters defined on the figure), which leads to a momentum $p = mv = eRB$. For a relativistic circular orbit, this relation is slightly modified in $p = eRB = \gamma mv$, then $\omega_0 = eB/(\gamma m)$ and $\omega_c = \gamma^2 eB/m$, and finally

$$\lambda_c = \frac{cm}{\gamma^2 eB}$$

Considering that at the ESRF, the energy of the electron beam is 6.03 GeV, that in a bending magnet the magnetic field can reach 0,4 T, we can have an idea of the magnitude of λ_c :

$$\Gamma = \frac{\mathcal{E}}{\mathcal{E}_0} = \frac{\mathcal{E}}{mc^2} = \frac{6.03 \cdot 10^9}{9.11 \cdot 10^{-31} \cdot (3 \cdot 10^8)^2} = 1.18 \cdot 10^4$$

and then

$$\lambda_c = \frac{cm}{\gamma^2 eB} = \frac{3 \cdot 10^8 \cdot 9.11 \cdot 10^{-31}}{(1.18 \cdot 10^4)^2 \cdot 1 \cdot 10^{-17} \cdot 0.4} = 3.1 \cdot 10^{-11}\text{m}$$

This new type of radiation is considerably much more intense than the cooling anode tube (up to 10 orders of magnitude more for a third generation ondulator at ESRF) [2]

2.2.2 Classical theory of X-ray scattering – bragg peaks

X-rays interact mostly with electronic clouds of atoms. In first approximation, an electron hit by an electromagnetic plane wave $E_0 = -A_0 e^{i\vec{k}.\vec{r}}$($\vec{k}$ wave vector) can absorb part of

this wave and reemit it in a spherical wave centered on the electron : $E = (A/r)e^{+ik'r}$; if the scattering is elastic, all the energy absorbed is reemitted, which yields $k' = |\vec{k}|$. Far from the electron, the wave is locally plane and we can write $E \simeq -(A/R)e^{i\vec{k'}.\vec{r}}$ where $|\vec{k'}| = |\vec{k}|$ and $\vec{k'}$ has the same direction as the observer.

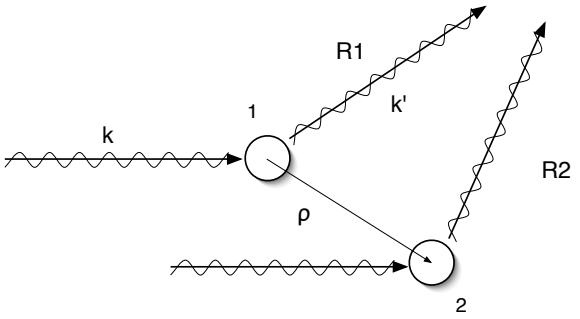

Figure 8: 2 scattering electrons
the wave arriving to these electrons is a plane wave. To calculate the resulting amplitude, one must considering the phase delay between two electrons for the re-emitted wave, but also for the incoming plane wave (calculi in text)

When there are two electrons, we have to consider that the initial plane wave may hit the second electron later than the first wave : the electron number 2 has a phase delay equal to $\vec{\rho}.\vec{k}$; on the other hand, at the arrival to the observer, another phase difference has to be taken into account due to the different length : the final amplitude at the observer will be :

$$E = -\frac{A}{R_1}e^{ikR_1} - \frac{A}{R_2}e^{ikR_2}$$

If $\vec{R_2}$ is expressed with $\vec{R_1}$ as : $\vec{R_2} = \vec{R_1} - \vec{\rho}$ with $|\vec{\rho}| \ll |\vec{R_1}|$ we have at the first order $R_2 = R_1(1 - \vec{\rho}.\vec{R_1}/R_1^2)$ which can also be written as : $R_2 = R_1 - \vec{\rho}.\vec{k'}/k$, and then if we take only the first order that will give constructive interferences in the resulting intensity, we have to assume $1/R_1 \simeq 1/R_2$ and we finally have

$$E = -\frac{A}{R_1}e^{ikR_1}\left[1 + e^{i\vec{\rho}.(\vec{k'}-\vec{k})}\right]$$

we define the momentum transfer $\vec{q} = \vec{k'} - \vec{k}$ and it gives $E = -A/R_1 e^{ikR_1}\left[1 + e^{i\vec{\rho}.\vec{q}}\right]$. For a large distribution of N electrons observed far enough for each inter-electron distances to be very small beyond the observer distance, we can generalize the previous expression[5] to :

$$E = -\frac{A}{R_1}e^{ikR_1}\sum_{i=1}^{N} e^{i.(\vec{r_i}-\vec{r_1}).\vec{q}} \tag{2}$$

Since the pre-factor $-A/R_1 e^{ikR_1}$ is of no significant importance importance in the intensity pattern, we will simplify the expression above in :

$$E = \alpha\sum_{i=1}^{N} e^{i.(\vec{r_i}-\vec{r_1}).\vec{q}} \quad .$$

It is possible to show [2] that the electrons of an atom can be averaged in a single scattering unit with a slightly difference : a factor, q-dependent, called "atomic form factor", that

[5] It has been assumed that the wave arriving to the first electron has the phase reference

changes with each type of atom. Then, the amplitude of a collection of atoms will be, in the same manner,

$$E = \alpha \sum_{j=1}^{N} f_j(\vec{q}) e^{i.(\vec{r_j} - \vec{r_1}).\vec{q}} \tag{3}$$

where j denotes the j^{th} atom.

Intensity diffracted for a crystal : if we consider a crystal, where atoms are periodically organized, we can arrange the above sum according to :

$$E = \alpha \sum_{p\ unit\ cells} e^{i.(\vec{R_p}).\vec{q}} (\sum_{j\ \in\ unit\ cell\ p} f_j(\vec{q}) e^{i.(\vec{r_j} - \vec{r_1}).\vec{q}})$$

where R_p is the position of the p^{th} unit cell. If we assume that the amplitude resulting from an unit cell is the same whichever the unit cell, we can change the sum above in :

$$E = \alpha A(q) \sum_{p\ unit\ cells} e^{i.(\vec{R_p}).\vec{q}}$$

where A(q) represents the factorized sum over an unit cell. Since the crystal is 3-dimensionally periodic, we can write R_p as a combination of the basic vectors of the unit cell : $R_p = n_1\vec{a_1} + n_2\vec{a_2} + n_1\vec{a_3}$.
Let's construct a vector basis $\vec{a_i^*}$ that satisfies $\vec{a_i^*}.\vec{a_j} = 2\pi\delta_{i,j}$ (i.e. each $\vec{a_i^*}$ is orthogonal to the plane formed by $\vec{a_j}$and$\vec{a_k}$ when $i \neq j \neq k$, and $|\vec{a_i^*}| = \frac{2\pi}{|\vec{a_i}|}$). If we decompose $\vec{q}$ in this basis (called the "reciprocal lattice"), we can write $\vec{q} = h\vec{a_1^*} + k\vec{a_2^*} + \vec{a_3^*}$ with :

$$(\frac{h}{a_1})^2 + (\frac{k}{a_2})^2 + (\frac{l}{a_3})^2 = \frac{q^2}{4\pi}$$

and $\vec{q}.\vec{R_p} = 2\pi(hn_1 + kn_2 + ln_3)$ which gives

$$E = \alpha A(q) (\sum_{n_1} e^{2i\pi h n_1}) (\sum_{n_2} e^{2i\pi k n_2}) (\sum_{n_3} e^{2i\pi l n_3})$$

we can easily calculate these sums :

$$\sum_{n=1}^{N} e^{i\gamma n} = e^{i\gamma} \frac{1 - e^{iN\gamma}}{1 - e^{i\gamma}} = \frac{e^{i\frac{N}{2}\gamma}}{e^{-i\frac{\gamma}{2}}} \frac{\sin(N\gamma)}{\sin(\gamma)}$$

Finally, if we approximate the crystal to a kind of parallelepiped (no complication on the crystal borders...), we can write the intensity, the squared modulus of the amplitude, as :

$$I = E^2 = \alpha^2 A(q)^2 (\frac{\sin(\pi N_1 h)}{\sin(\pi h)})^2 (\frac{\sin(\pi N_2 k)}{\sin(\pi k)})^2 (\frac{\sin(\pi N_3 l)}{\sin(\pi l)})^2$$

with N_i the number of unit cells in the i^{th} direction.
it will be studied further that the function $f(x) = (\frac{\sin(\pi N x)}{\sin(\pi x)})^2$, called the "network function", has small oscillation close to 1 except in the vicinity of sharp peaks situated at

$$x = n \in Z$$

It results that a significant intensity will be delivered when **h, k or l are integers** . Each diffraction peak is then indexed by three integers, h,k and l, named the "Miller indices", and we will label the corresponding distance (or momentum, or angle) by $d$hkl (respectively $q$hkl and θhkl).

Intensity diffracted by a fluorohectorite particle: let's consider a unit cell of fluorohectorite : two unit cell vectors are given by the hexagon periodicity in the platelets (see fig. 2), while the stacking direction gives the last vector.

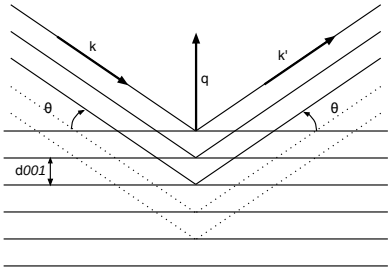

Figure 9: schema of Bragg's diffraction planes
the momentum transfer $\vec{q}$ is parallel to the stacking direction and its value is $q = n\frac{2\pi}{d}$

If we take $h = k = 0$, we will have diffraction for $l \in Z$, i.e. when $\vec{q}$ **is parallel to the stacking direction** and $q/2\pi = l/d001$: this mean that, since the scattering is elastic, the incident and refracted beam form the same angle theta with the sheet plane, angle determined by the **Bragg's law** :

$$2d001\sin(\theta) = n\lambda \quad n \in Z \tag{4}$$

Implicitly, we used the equivalence between q and $theta$; we also can define a new parameter, "d" (not to be confused with "$d001$"), like following :

$$q = \frac{2\pi}{\lambda} = \frac{4\pi}{\lambda}\sin(\theta)$$

Braggs law can then be expressed very simply with the d parameter :

$$d = \frac{d001}{n} \quad n \in Z$$

2.2.3 Equivalence between network and lorentzian function

In a one-dimensional problem of scattering of a collection of N periodic objects, we usually obtain in the resulting intensity a factor which is the Network Function :

$$\Phi = \frac{\sin(\frac{N\xi}{2})^2}{N\sin(\frac{\xi}{2})^2}$$

with $\xi = q.a$, where q is the momentum transfer and a the distance between scatterers. This function gives a lot of oscillations but with much more intense peaks at positions $\xi_n = 2n\pi/a$. When N grows towards infinity, this function evolves into a periodic sum of diracs centered on each of these qn. However, before reaching this limit, we still have some oscillations of relative importance near each peak that gives the impression of a "tail" of the peak. Let's consider the position of each maximum close to the peak at $\xi = 0$: these maxima satisfy the equation $\frac{d\Phi}{d\xi} = 0$ which leads to

$$\tan(N\xi) = N\tan(\xi)$$

Considering the fact that N is great (more than 100), the function $\tan(N\xi)$ is, in first approximation, null when $\xi \neq \frac{(2m+1)\pi}{N}$, which gives maxima positions at $\xi_m = \frac{(2m+1)\pi}{N}$.

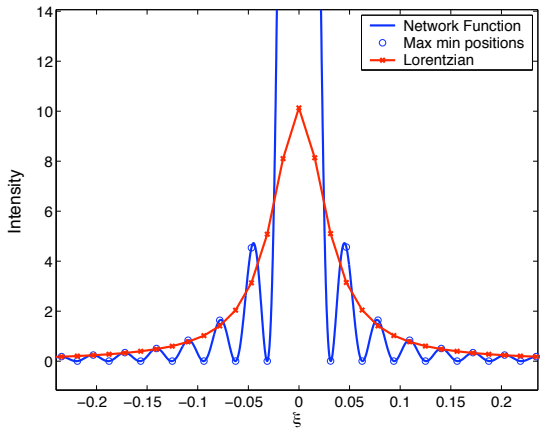

Figure 10: Lorentzian-Network comparison for $N = 100$ and $a = 1$; formulas in text
we plotted the network function, emphasizing its maxima, and the lorentzian function to see it coinciding after the third maximum.

But for the first few m, we have $m << N$ and then $\xi_m << 1$, then $\sin(\xi_m)^2 \simeq \xi_m^2$: the decay of maxima around the peak is in $1/\xi^2$, with an intensity of $\Phi(\xi_m) \simeq \frac{N}{((2m+1)^2\pi^2)}$. This is why we can fit the tail of the peak by a Lorentzian peak function [4] : a normalized lorentzian is described by the equation

$$Lo(\xi) = \frac{1}{\pi\Omega_L(1+\frac{\xi^2}{\Omega_L^2})}$$

and if we report the maxima positions in this equation, it gives an intensity of $Lo(\xi_m) = \frac{1}{\pi\Omega_L(1+\frac{(2m+1)^2}{(N^2\Omega_L^2)})}$; if we take a Ω_L close to $\frac{1}{N}$ (remember that we want to fit a peak that have a $\frac{1}{N}$ width), then when m is large enough (practically, it occurs already for m greater than 3) we have

$$Lo(\xi_m) \simeq \frac{N^2\Omega_L}{\pi^3(2m+1)^2}$$

which is equivalent to the original Φ function that we want to fit on the condition that we take

$$\Omega_L = \frac{\pi}{N} \quad .$$

2.2.4 Fit limitations

Several physical effects have some bad effects on this fit. First, we can see that the Lorentzian does not fit the height of the network function. On the other hand we have to consider several other effects that make the final shape of these peaks different from this network function :

- First there is a size distribution, pretty large for fluorohectorite, that attenuates the contrast between these maxima and minima by smoothing the network curve
- Fluctuations in inter-lamellar distance can also smooth a lot the pattern and give a single peak instead of a peak with a lot of side-fellow peaks

But the most important limitation is the instrumental resolution : under this appellation are hidden effects such as non monochromaticity or divergence of the beam that turn the signal to be the sum of each signal produced by a single wavelength or a single incident angle, and pondered by a density of probability. We can assume that each of these density are gaussian, and then the result is a multiple convolution between the signal and several gaussians, that can be reduced to a single gaussian called "instrumental resolution" : $\Phi(q) = \int \Phi_0(q-s)G(s)ds$ where G is the gaussian we talked about. For our signal, Φ_0 is a lorentzian and G a gaussian, and the resulting convolution is called a Voigt function. It is classically [16], [8] approximated with a Pseudo-Voigt function with an identical width. That width, as well as the weight of each of the functions in the sum, are related to the widths of the original gaussian and lorentzian, according to :

$$\Phi(q) \simeq \frac{\eta}{\pi\Gamma(1+\frac{(q-q_c)^2}{\Gamma^2})} + (1-\eta)\sqrt{\frac{\ln(2)}{\pi\Gamma^2}}\exp(-\frac{\ln(2)(q-q_c)^2}{\Gamma^2}) \tag{5}$$

where Γ and η are estimated as :

$$\Gamma = (\Omega_G^5 + 2.6927\Omega_L\Omega_G^4 + 2.4284\Omega_L^2\Omega_G^3 + 4.471\Omega_L^3\Omega_G^2 + 0.078\Omega_L^4\Omega_G + \Omega_L^5)^{\frac{1}{5}} \tag{6}$$

and

$$\eta = 1.366\frac{\Omega_L}{\Gamma} - 0.47719(\frac{\Omega_L}{\Gamma})^2 + 0.11116(\frac{\Omega_L}{\Gamma})^3 \tag{7}$$

We practically obtain Ω_G when we calibrate the distance to the detector with Si single-crystal powder, which produces bragg peaks at a given angle with a much smaller width that the instrumental resolution. Then we can obtain Ω_L by numerically reversing equation 7 [6].

3 Experiments

3.1 Samples

The work done in this internship does not includes sample preparation : the samples we used were prepared in 1999 by S.B. Lutnæs [10], and in 2000 by M.W. Haakestad and T.N. Aalerud [7] [9], [1]. The exact protocol for sample preparation is readable on these persons' master thesis, and is not really our purpose. However, since these thesis are not easily available, and since the protocol may be responsible for some effects we observe, here is a summary of the main steps followed in sample elaboration.

1. Dissolution in water :
   fluorohectorite powder is dissolved in distilled water, with a pH adjusted to 10 for Lutnæs samples, and the solution is stirred with a magnetic stirrer for 1 day (4 weeks for 10t samples). After that, some salt containing replacing cation (Mainly Li, Fe,Ni and Na) is added to the solution

2. Dialysis
   The solution is left for a while (several days) and then is placed inside a dialysis set-up to get rid of Cl^- ions ; for 10 t samples, only part of the sample is taken after a phase separation. Once there are no more excess ions in the suspension, we can basically assume that there are only the salt cations in interlayer spaces

[6] this polynom has hopefully only one root

[7] these two types of samples have been named "Lutnaes" and "10t" throughout experiments, and so shall we do in this report

3. Drying
   Finally, the cation-exchanged samples are re-dispersed in deionized water and subsequently dried out under a constant uniaxial stress. For that, a press has been used with several loads (from 50 kg for "Lutnæs" samples to 10 t for "10t" samples

This procedure has 3 goals :

to produce clean samples of fluorohectorite with different interlayer cations

to produce dried solid sample in order to manipulate them easily in diffraction experiments

to align more or less the fluorohectorites perpendicularly to the pressing direction.

This preparation produces samples of several mm thick with an orientational distribution that clearly enhances the direction perpendicular to the sample, as it can be seen in x-rays rocking scans : we place the sample and a single-point detector at the position of a bragg peak, and then we rotate the sample only : because only well-oriented particles are able to scatter non negligible intensity, it gives an idea of the particle orientation distribution. This is mainly a gaussian with a half width of 30° for 10t samples and 24° for Lutnæs samples[8].

3.2 TGA

3.2.1 Overview

The goal of these experiments is to measure mass variations during hydration or dehydration of clay powders. We use for that a Mettler-Toledo thermogravimetric analyser (TGA/SDTA 851e-LF-1100), able to record mass variation with an uncertainty of 10e-6 grams while ensuring a temperature around the sample in a range from 25°C to 1100°C. An alumina crucible filled with clay powder is put on the balance and an interactive software imposes temperature variations while at the same time an external humidity reservoir (a salt saturated solution) imposes relative humidity to the thermodynamic system.

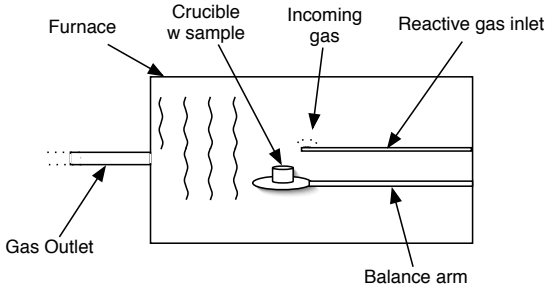

Figure 11: Schema of the TGA
the sample is put in a crucible on the balance arm of the device, and the furnace slides to surround the sample and ensure a controlled temperature

[8] surprisingly, the samples that were the less pressed are the more aligned perpendicularly to the pressing direction. There is no explanation for that in the moment.

3.2.2 Improvements

The original set-up of the TGA was made with a single bath with cooling liquid, used for both furnace and balance measurement cell. Since the original firmware of the device had a security preventing the use of the TGA for temperatures below 25C, the company Mettler-Toledo sent us a new firmware able to avoid this limitation, under condition that we use two thermostated baths, one for the furnace and one other for the measurement cell. We have also made a better humidity control system (the old one had many leaks) that improved the humidity inside the furnace, specially for wet air, and we thus were able to reach relative humidity such as 97% or 6%.

3.2.3 Protocol

We used the TGA to record mass variations during heating or cooling processes. Since there is an hysteresis in the hydration transition we mainly measure the mass variations in only one "direction" : the main protocol have then been to heat the sample until total dehydration, or to cool the sample until total hydration (we must be careful to avoid condensation though), usually during a whole day and night, by temperature steps of variable length. The samples we used are powder of Ni-,Li-,Na- and Fe-fluorohectorite. For each of them we took an amount around 3 grams, to reduce as much as possible any effect of delay due to diffusion in the sample;

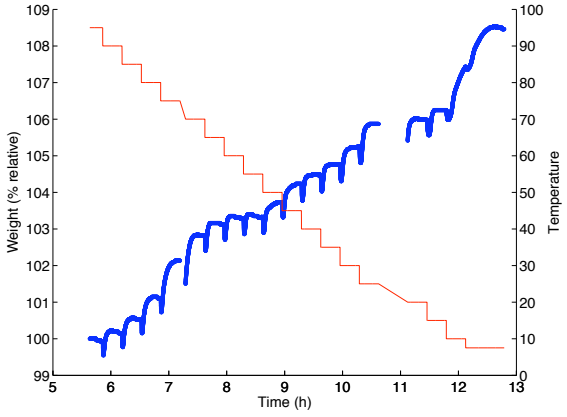

Figure 12: Weight variation with temperature for FeFLHC.
Rough TGA data have characteristic artifacts in the beginning of each temperature step : the sudden change of temperature in the furnace perturbs for a short moment the balance which measure less than the final mass of the previous step . Bold : relative weight ; thin : temperature

Unfortunately this made our signal very noisy, in particular when Temperature is changing : we discovered, by performing blank curves, that the balance is (unwillingly) very sensitive to heat fluxes and produces large overshoots when temperature changes. We then decided, when possible, to subtract a blank curve to each of our signals; this subtraction, as well as every other calculus and fits, have been performed on Matlab after having exported the datas from the Star software. This was not possible though to do on each of the recordings; in these cases we treated the rough datas. The treatment consists in an exponential fit : for each temperature step, we fitted with the formula $m = Ae^{-\lambda(t-t_0)} + m_{\text{end}}$. The results to be produced were then the variations of m_{end} with the step temperature, since m_{end} is the closest value to the thermodynamic final equilibrium under these conditions. The other parameters of the fit, are not that relevant, specially because of the heat fluxes perturbations on the balance (as explained before), and contrary to the final

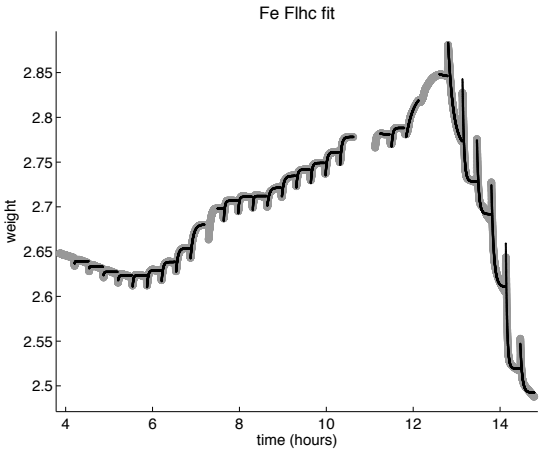

Figure 13: exponential fit
here is what we obtain by fitting the data with exponentials.Bold gray: relative weight data ; thin black : fit

mass, even after substraction of a blank curve, the masses at the beginning of each step (on which are fitted the most the A and λ parameters) are not reliable.

3.3 X-ray scattering

The aim of these experiments is to shoot 2D pictures of a X-ray scattering pattern during the water intercalation process in fluorohectorites clays. The source being used comes from the Swiss-Norwegian Beam Line (SNBL) in the European Synchrotron Resource Facility (ESRF-Grenoble).

3.3.1 Experimental cell, Temperature and Humidity control

The cell we use for X-ray scattering have been designed to be X-ray permeable as well as impermeable to air (to impose humidity) and thermally isolated to avoid temperature gradients. The covers of the cell are made of beryllium because this metal has a very low absorption coefficient for X-rays : it fulfills the conditions demanded above. Samples are mounted on copper blocks in which are a thermistance and a Pelletier element heating the air circulating through a copper foam, which gives a better thermal contact than solid copper, this to avoid large temperature gradients inside the cell. The lower face of the pelletier is kept at constant temperature with a thermostated bath while the other side can be used for heating or cooling, and the final adjustments are made by the thermistance linked together with a thermocouple to an auto-tuning temperature controller. This controller has a PID controlling system that allows to keep a temperature for days with a 0.1°C uncertainty only. At the same time, a varistaltic pump supply air in which humidity is imposed by salt-solutions reservoirs to the inside of the cell, and humidity is measured just upon the sample by a sensor fixed in the covers.

3.3.2 ESRF set-up

The X-ray beam provided by the SNBL is a 0.5mm square large x-ray beam with a wavelength of 0.8 Angstrøms. This beam goes straightly to the cell fixed on a goniometer, and a mar345 photon detector, situated around 30 cm further, is used to record the 2D X-ray

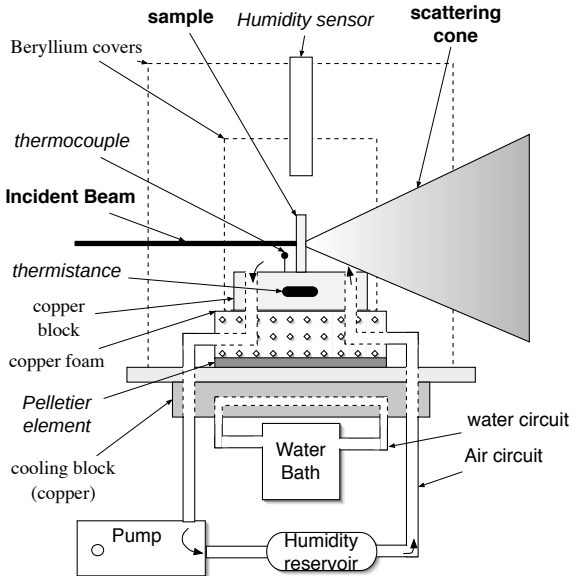

Figure 14: Schema of the experimental cell.
here is presented the experimental cell we used for X-ray diffraction. Sample holder as well as the support for goniometer axis were made for these experiments.

diffraction pattern. But Before any measurement we need to calibrate the detector, i.e. to know precisely what is its distance to the sample. For that we use Si-crystal which produces very narrow peaks at very well-known positions and then we are able to relate each point of the detector to a scattering angle. Once this is done, each measurement is

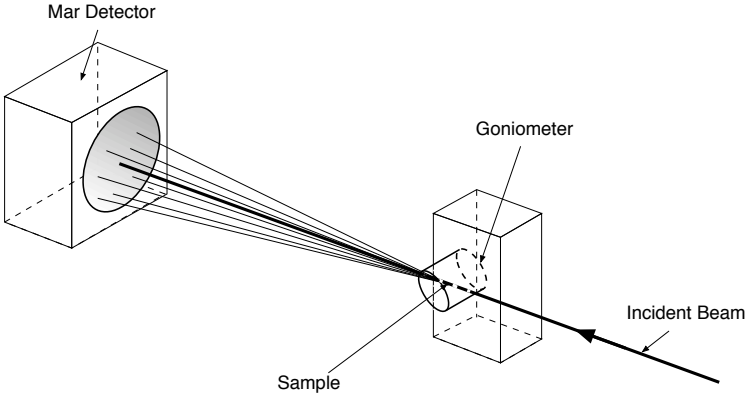

Figure 15: Schema of the experimental set up
The goniometer allow rotation of the samples and the mar detector records the diffraction pattern.

taken from the control room where several softwares enable to manipulate the beam, the detector and the temperature controller. In order to control the temperature from the control room, a Labview software has been designed to control the auto-tuning temperature controller (see Annex), but since there was no plug in the hutch fitting the output of the device, we had to use the labview program on a laptop controlled from outside with a Windows Remote Desktop.

3.3.3 Protocol

The main idea of our protocol was to record diffraction patterns during hydration transition to see the in-plane peaks moving (or not) and to determine the water layer. Then it has been chosen to first heat the sample in dry conditions to get rid of the water, and then to cool it down under wet atmosphere. Though, because of the limited time we had, it has been often chosen to change what we originally planned to do and then, it is quite difficult to define a clearer protocol.
We used six samples, two Na and one Ni "Lutnæs" samples, one "10t" Na sample, all of them pressed samples, and two other powder samples, one Li and one Fe. apart from the first Na sample, who stayed one day and a half because of all the final set-ups (avoiding shadows, etc.), each sample has stayed around 18 hours in the cell.

4 Discussion

4.1 Thermodynamic characterization of transitions

Here are the fitted results for Ni and Fe fluorohectorite.Fig 16 represents the relative weight variations in the sample.

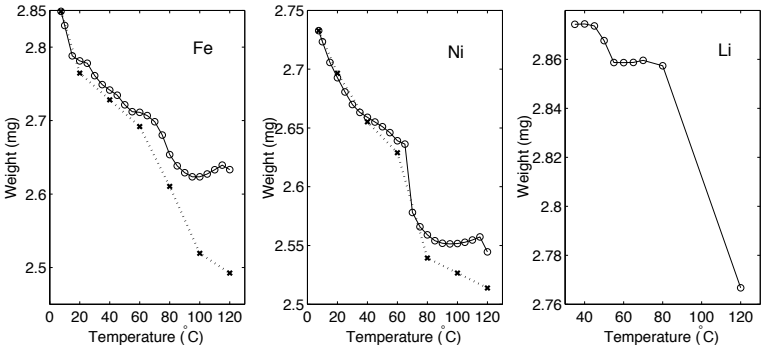

Figure 16: fitted equilibrium weight with temperature
These are the final fitted weight for each temperature step; circles : slow cooling ; crosses : fast heating

We have several remarks to do on these curves : first, each of them have a characteristic loss of weight during the first steps of cooling : between 120 and $100°C$, the weight of each sample, instead of increase because of wet-cooling atmosphere , continues to decrease. This can be explained with two arguments :

- first, for a same relative humidity, the real water pressure is less important at high temperatures and then we may be at a temperature range where temperature variations have little effects on the sample, which means that for stable equilibrium states, the mass variations would be negligible.
- then, we know that in the macroscopic point of view, dehydration for smectites may have at least two processes (maybe more), like interlamellar dehydration (which is what concerns us) and also mesoscopic dehydration, due to mesoporosity. [5] We know that this second process have a much more longer time constant, and induces mass variations that are lower than interlayer water absorption, but not that much (around 10%). the final reason for this mass decrease could be then only kinetic, due to the slow evaporation of water in mesopores, an effect that stops when the sample reach $100°C$.

For lithium and sodium fluorohectorite, we see clearly two hydration occuring, one around 80°C and the other around 50°. (for Na-FLHC, see C.Coussa internship report[5]) For nickel and iron fluorohectorite, a first important gain of weight occurs around 85°C for Fe and 75°C for Ni. This is certainly due to a first water layer entering the sample. For lower temperature, things are less clear : weight increases slowly and irregularly ; it could mean that water molecules settle the mesoporous spaces, but the weight gain is, in the end, too large in comparison to the mesoporous volume ; an other possibility is that this slow increase is in fact the slow addition of a second water layer, but with several steps in between with only a "half of layer" that could correspond to a stable or metastable arrangement of inter-layer water molecules in an amount that could be 1,5 times the amount of what we called "one water layer". This effect is less clear for nickel, and inexistent for lithium and sodium, where we see clearly two hydration steps. This is probably due to the cation size and valence, much higher for nickel and iron than for sodium or lithium : a higher valence allow larger possibilities of cation-water molecule arrangements.
Finally, we see a last important gain of mass around low temperatures ($T < 15$°C, so-called "low" because close to the ice crystallization temperature). This mass increase is to be taken as addition of an other water layer because the mass gain is around the same amount of water than for the first water layer. Another important effect is that curiously, Ni and Fe samples seem to lose much more mass in the last heating than in the first heating (the first point on the curves), which however lasted more time. An explanation could be that there is some aging process that make water initially present in the sample (because of humidity of ambient air) more difficult to remove than after mixing with some "new" water, that did not reach yet the spatial configuration with the lowest energy. In the table 1 are situated the characteristic transition temperatures for Li, Na, Ni and Fe powders and in table 2 the equilibrium masses.

Fe	transition	cooling temperature	heating temperature
	0wl-1wl	90°C	80°C
	1wl-2wl	25°C < T < 55°C	25°C < T < 55°
	2wl-3wl	15°C	10°C
Ni	transition	cooling temperature	heating temperature
	0wl-1wl	70°C	60°C < T < 80°C
	1wl-2wl	35°C < T < 55°C	35°C < T < 55°
	2wl-3wl	7.5°C < T < 35°C	7.5°C < T < 35°
Na [5]	transition	cooling temperature	heating temperature
	0wl-1wl	65°C	90°C
	1wl-2wl	45°	25°C
Li	transition	cooling temperature	heating temperature
	0wl-1wl	80°C	90°C
	1wl-2wl	50°C	60°C

Table 1: Transition Temperatures

4.2 Localization of Hydration transition in WAXS data

4.2.1 Characteristic spectra

Because of randomly orientation of FLHC particles in the sample, the mar pictures shows intensity rings that have to be integrated to get a spectrum (see apendix). For that we

Sample	0WL	1WL	2WL	3WL
Fe	2.623 mg	2.712 mg	2.788 mg	2.850
Ni	2.551 mg	2.636 mg	2.663 mg	2.733
Na [5]	13.2 mg	13.55 mg	14.35 mg	-
Li	2.767 mg	2.858 mg	2.878 mg	-

Table 2: equilibrium masses

use the Fit2D[9], a software that can analyze X-ray scattering data and perform picture treatment such as circular integration (the only treatment that we wanted to do for now). We performed these integration with some perl scripts [10] that uses parameters such as the detector's distance, the center of the beam (determined with the Si-single crystal samples) and polarization of the beam to produce the spectra of all pictures with a normalized intensity in order to supperpose these spectra and compare them.

At this moment we were able to look at the intensity diffraction pattern plotted with only one parameter (d,q or 2θ) which was necessary to look closely to each sample to see transitions occuring. A single spectrum (fig. 17) shows several peaks that have to be interpreted to give significant explanation. By comparison to the background, shown in

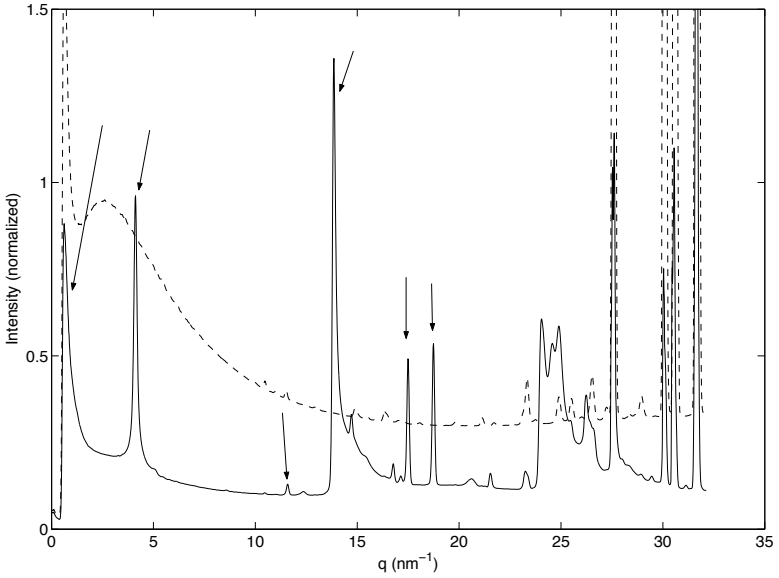

Figure 17: example of diffraction spectrum for Na-FLHCThis spectrum is rather complex : a lot of peaks does not really correspond to the sample, which make identification uneasy.plain line : NaFh spectrum ; dashed line : empty cell background ; arrows : explained in text.

dashed line, we can discriminate which peaks really come from the clay sample and which others are due to beryllium. Some of these peaks are showed with arrows and will be commented from the left to the right.

1. This arrow shows the small-q peak. This peak is due to the fact that most of the

[9] http://www.esrf.fr/computing/scientific/FIT2D/
[10] gently provided by Y. Méheust

incident beam is transferred straight away, when q goes to 0. This peak can show larger-scale effects, like how the clay particles are organized together, but it cannot be analyzed here and requires specially-designed setups analyzing for example the power-like decrease of the low-q region of the spectrum (small-angle scattering). However, for data obtained with a wide-angle scattering, this part of the spectrum is not relevant because the resolution is not the best, and also because in the experimental set-up, the direct beam is stopped with a lead circle sheet to avoid damaging the detector.

2. The second arrow is around $q = 4,12\text{nm}^{-1}$, which correspond to $d = 15.25$Å. This distance is exactly the d001 distance, i.e. the stacking distance, for a 2 water layer NaFLHC sample [7]. This is the case l=1 if we take the notations from the previous chapters. These peaks can move a lot during hydration transitions, from $d = 9$Å to $d = 15$Å ($q = 7.0\text{nm}^{-1}$ to $q = 4.1\text{nm}^{-1}$), but as we can see, there are no other peak in this range that could interfere in our interpretation. These peaks are those that will be used to determine the hydration state in each sample, because they show the inter-layer distance. The difficulty, as will be explained later, is during transition when some of these peaks will be present at the same time.

3. The third arrow is at $q = 11.6\text{nm}^{-1}$ which correspond to $d = 5.4$Å. This is around twice the O-O distance in the hectorite Si04 tetrahedron [4], which is the periodicity of in-plane hectorite unit cell. this is probably due to OH remaining from the F replacement in Fluoro-hectorite production.

4. The fourth is around $q = 13.85\text{nm}^{-1}$ which correspond to $d = 4.53$Å. This should be, according to the importance of these peaks, twice the real O-O distance in fluorohectorite. We remark also that this peak has a very strange shape : it increases very sharply and decreases quite slowly ; this is probabely due to the superposition of several other peaks, like the one for the case h=1,l=2 which gives a peak at $q = 14.22\text{nm}^{-1}$. There could be also the fact that the intercalated water takes specific places around intercalant cations (skipper) and for that gets also a periodicity, the same as in-plane peaks , but very noised, that would gives a very large peak to add to this; finally, as we can see, as we can see, a peak around $q = 14.8\text{nm}^{-1}$ comes also from the background in this region.

5. The next peak is not explained for the moment

6. The next and final peak is at $q = 18.75\text{nm}^{-1}$ and can be linked to the case $h = 1, l = 3$ that gives $q = \sqrt{13.8^2h^2 + 4.12^2l^2} = 18.60\text{nm}^{-1}$. However this is not a very satisfying explanation.

After having pointed which peaks correspond to what, we have to determine when do transitions occur in order to determine which patterns correspond to what hydration state. An example of transition is given in figure 18, though other graphs are shown in appendix.
When we have patterns like those shown in fig. 18, we have to look carefully to the distances involved, but also to the sense in which the transition evolves, particularly when the peaks abscissae do not correspond to ideal hydration states because of some shift (see below) in the peak.

4.2.2 Transition temperatures

Table 4.2.2 shows the temperature ranges in which transitions occurred. These ranges are quite large because temperatures variations were sometimes faster than the transition

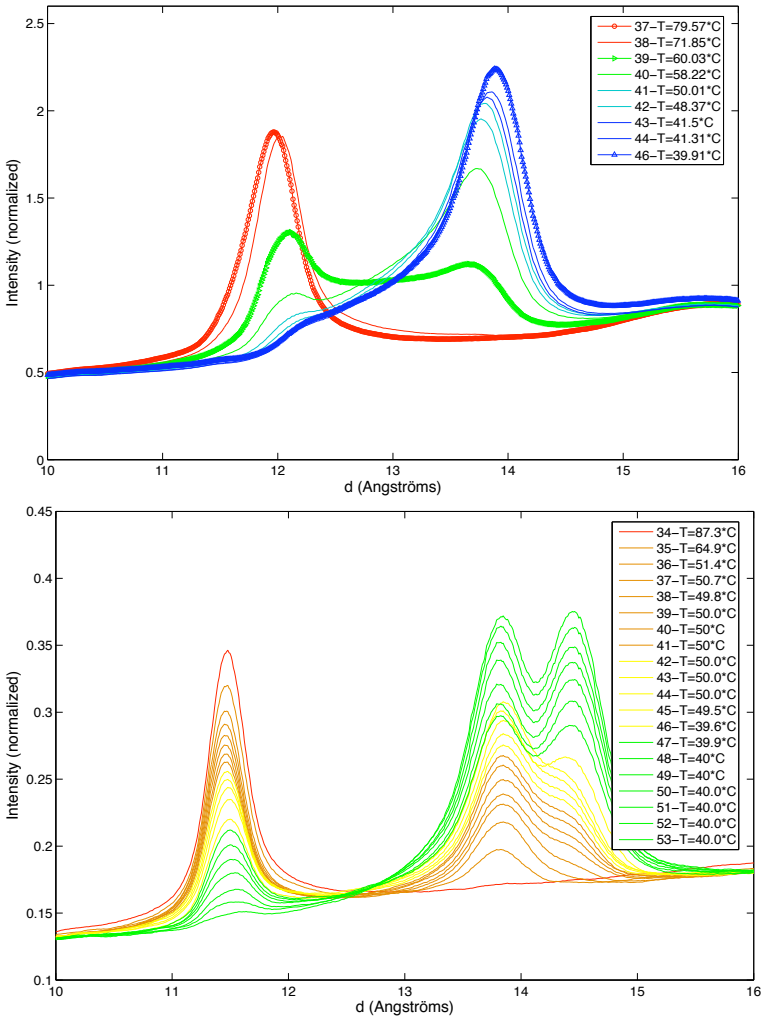

Figure 18: diffraction pattern of hydration transition.
As we can see, each peak is asymmetric during the transition, and the peaks are slightly shifted (when it is not a single peak that moves along the d-abscissa).
Up : FeFlhc 1WL-2WL ; down : NiFLHC 0WL-1WL

itself. This table has been made just by noting the temperature on which transitions were occurring and comparing the d001 distances to some references for Ni and Na. The fact that there are no references on Fe and Li distances makes the results on these samples less precise, and we cannot be really sure of what is the water layer level we observe, except by comparison to Na and Ni samples.
There are a few things that have to be explained in the table : first, we have not been able to see all the hydration transitions of each sample, which explain some of the interrogative points; there were also some transitions between two peaks that happens to have approximatively the same hydrations state but with some different d001 length : that explains why some times there is written 1wl-1wl or 2wl-2wl transition; we also had, as said before, some problems of diffusion delay time longer than our temperature variations, which explains sometimes very large ranges for a temperature, and specially for Fe.

Fe	transition	cooling temperature	heating temperature
	0.5wl-1wl	100°C <Tc01< 120°C	100°C <Tc10< 120°C
	1wl-2wl	40°C <Tc12< 100°C	60°C <Tc21< 100°C
	2wl-2wl	40°C <Tc12< 100°C	60°C <Tc21< 100°C
Ni	transition	cooling temperature	heating temperature
	0wl-1wl	64.9°C <Tc01< 120°C	40*C<Tc10<120*C
	1wl-1wl	40°C <Tc< 64.9°C	??
	1wl-2wl	15°C <Tc23< 40°C	??
Na	transition	cooling temperature	heating temperature
	0wl-1wl	100°C <Tc01< 120°C	100°C <Tc10< 110°C
	1wl-2wl	40°C <Tc12< 100°C	60°C <Tc21< 100°C
Li	transition	cooling temperature	heating temperature
	0wl-1wl	92°C <Tc01	120°C < Tc10
	1wl-2wl	0°C <Tc12< 25°C	0°C <Tc10< 40°C

Table 3: Transition Temperatures

4.3 Out of plane peaks fit

Once the integration spectrum are made, we have to fit the peaks in order to know precisely their position. The fit itself consider a background to remove, and fits the resulting data with a Pseudo-Voigt function, as explained upper in the text, considering other factors in the intensity (such as the unit cell form factor, A(q), constant in the peak range) to finally output the Pseudo-Voigt fitting parameters such as η, Γ, Ω_L and q.

4.3.1 Pure state characterization

Several results have to be interpreted for the four samples we used. All the out of plane peaks corresponding to pure states have been plotted in figure 19. We can see first that for samples with monovalent cations like Na- , the pure states are well defined : we have clear d-spacing corresponding to these pure states, and that are in good agreement with previous studies on these samples [6]. However the Li-sample is less clear but this is due to the protocol : we went too fast with temperature, which induced a sort of delay and then we miss some of the pure states.
Samples with polyvalent cations, like Ni and Fe are, on the other hand, harder to understand, because a lot of peaks seem to correspond to pure hydration states, but are too close to each other to be taken as well and the transition from one to the other is more a single peak shift than two peaks interacting. An interpretation could be to see it as some sort of spatial rearrangement of water molecules between the platelets (cf skipper). Tga data show that for these kind of cations, there can be a sort of "slow weight gain" and maybe this could be due to a slow absorption of water, by small amounts, that does not really change the inter-layer amount of water but which integration in the layer requires a different spatial arrangement [13], so different that it could produce different d001 distances. If we compare the distances obtained for Ni to those obtained in previous studies [1] , two peaks that seem to be pure hydration states correspond to only one water layer, while the peak corresponding to the longest distance seems to be 2WL. If we compare these results to those we have for Fe-FLHC, and specially the fact that some peaks are shifted into another, we may assume that Fe-flhc behaves the same as Ni-flhc, and that there are some rearrangements of inter-lamellar water in the 2WL hydration state. The table 5 resumes all the hydration states and their corresponding distances, as well as the

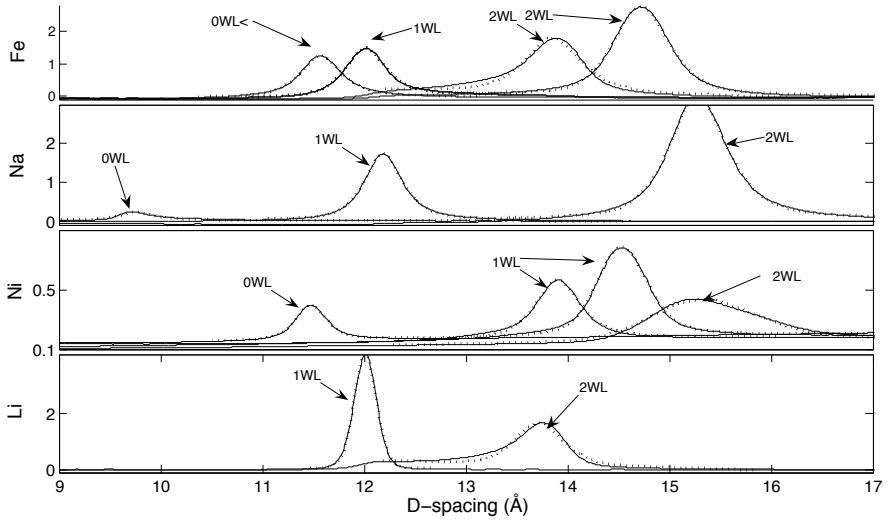

Figure 19: Pure hydration states for Fe,Na,Ni and Li samples.
Here are the peaks with the thinnest width that were assumed to be the closest to pure hydration state.
Plain line : data ; dashed line : fit.

stacking size calculated with the lorentzian width : $N = \frac{q}{\Omega_L}$ [17]

Table 4: Characteristic hydration distances

Hydration state	0WL	1WL	2WL
Fe	<11.4 Å	11.53 Å	13.85Å to 14.7 Å
Na	9.76Å	12.2 Å	15.28 Å
Ni	11.46 Å	13.87Å to 14.53Å	15.2 Å
Li	???	12.03 Å	>13.8 Å

The number of stacking platelets obtained seems to be in agreement with previous results [7], except for some anomalies : for lithium, the number is quite large. This may be due to the fact that on the spectra, this sample showed peaks that looked pretty much like gaussians rather than Pseudo-voigt (the parameter η, defined previously, was very small). However it is not impossible that lithium induces a greater size of fluorohectorite particles. Another anomaly is the very low number of particles for Ni this may be due to the fact that the peak that was taken for 2WL was slightly perturbed because the transition was not fully achieved, which can make the peak larger.

4.3.2 Hydration Transitions

Transitions are much more difficult to characterize than pure state, specially because the resulting spectrum is not at all a pondered sum of pure state spectra. During transitions, there is a phenomenon called "mixed intercalation" which means that incoming water does not full one particle after another : during the transition, there is a probability p for each inter-lamellar space to host a given number of water layers, and the resulting intensity is a very complex formula that involves the equilibrium d001 distances and these probabilities.

Table 5: stacking size (nb of platelets)

Hydration state	0WL	1WL	2WL
Fe	?	120 ± 10	110 ± 10
Na	60 ± 30	115 ± 5	65 ± 5
Ni	95 ± 5	60 ± 10	20 ± 5
Li	???	250 ± 15	??

This formula results from the Hendricks-Teller fomalism and does not enter in this report. Besides, due to the finite size of the scattering volume, different scatterers are in a different state of mixed-intercalation, so that the observed broad peak is a superimposition of many different Hendricks-Teller states [12]. However, the limit of this formula when p=1 or p=0 should be something equivalent to the network function, which means that in the beginning and the end of a transition, the peak is fitable with our previous pseudo-voigt formula without too much uncertainty. Here are the results of the fits on all our data : The

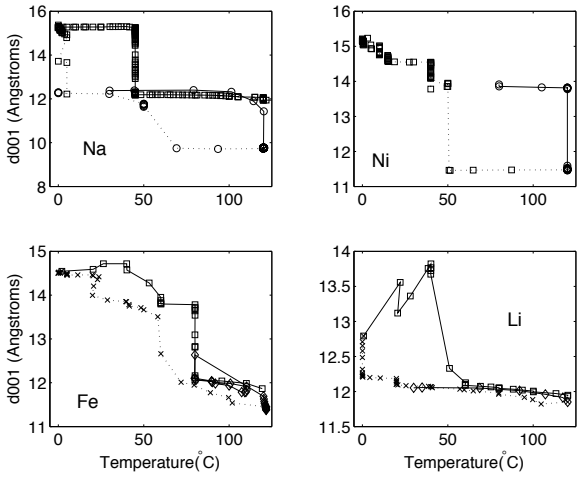

Figure 20: fitted position of d001 peaks during transition for Ni, Na, Fe and Li fluorohectorite.
the variation with temperature is not very clear : this is mainly due to transition delay we had in our samples; for example, FeFLHC presents a d001 smaller for T=0°C than for T=40°C where it is maximal, which cannot be explained without considering diffusion in sample and fast heat variation.
Plain line : heating ; dashed line : cooling.

fit used was made to fit the maximal peak (in the case of two peaks during a transition). Then we see that for Na fluorohectorite, there are two distinct peaks because as we see at 120°C and 40°C (two temperatures on which we stayed a lot during experiments), there is a whole space range where there are no data. But for nickel and iron, we can see both a clear step like for Na, and a slow variation for temperatures less than 50°C :this is the same behavior than for TGA data : there is a slow water intercalation. We have to notice that these pictures show the delay in transitions for this sample : for Fe FLHC, we can see that the highest peaks are around 40°C which is due to a (too) fast change of temperature : the 0°C previous step was too short : the sample was just beginning the transition when the temperature reached 40°C. This effect is much more clearer for Li sample, where temperature changes were so fast that we have only one single peak.

4.4 In-plane peaks

As explained before, one of the goals of this study was to detect movements in the in-plane peaks during Hydration transitions. The hypothesis was that during transition, water molecules coming between platelets could, by thermal agitation, and before having found its equilibrium position, hit fluor and make them move from the original position to (in average) thrust them deeper into the platelet, which could have the effect of contracting the unit cell and then make the in-plane peak move slightly. This hypothesis was found in literature [15] and observation on previous data showed a slightly change in the main peak abscissa. However, we have not been able to see them move in our study : fig 21 shows the position of the peaks maxima for all our data (pure states as well as hydration transitions)

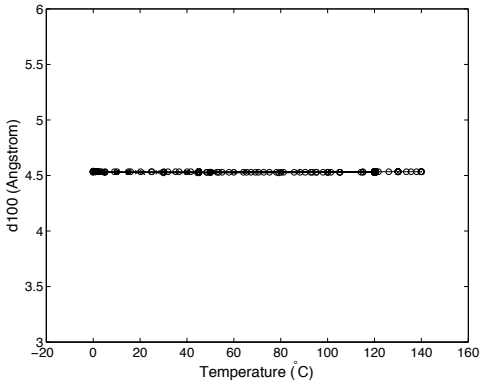

Figure 21: In-Plane peaks maxima position vs temperature.
obviously, there is no variation at all.circles : Na-FLHC ; crosses : Ni FLHC

Several explanations are possible :
First of all, our resolution may be responsible for that : the peak abscissa may have moved by a value as the same magnitude than our uncertainty on peak position (0.03nm^{-1}), but this is very doubtfull because the uncertainty in d corresponding is $e_d = 0.01$Å, a distance lower than the thermal mean square displacement...
then there may be an other explanation : the peak called "in-plane peak" is in fact a complex assembly of several peaks, which explains its asymmetric shape, and while the maximum, corresponding to the "real" in-plane peak (i.e. issued from the in-plane periodicity of crystal unit cells in a platelet), others peaks, such as multi-Miller indexed peaks (101, 102,...) may move because of the moving of the 001 peak, and this makes the resulting shape of the whole peak evolving.

Fig 22 shows how this in-plane peak evolves for Na-Flhc[11] (and Ni in annex). As we can see, peaks for 2WL are thinner and higher than for the other hydration states. Table 4.4 shows the distances (in q) for several peaks :
The 101 peak is exactly on the asymmetric tail of the peak we are studying, and may be partly responsible for this shape : as it can be seen on fig22, when the 101 peak is very close to the 100 (2WL), the whole in-plane peak is thinner and higher.But when the 101 peak a little bit further (1WL) the asymmetric part is more pronounced and the maximum is lower than for 2WL. Finally, when the peak is much further (0WL), the q100 peak becomes thinner again, but not higher, and the 101 peak becomes more visible.

[11] since two different Lutnæs samples have been used, we represented the common 1WL state in order to see which are noise peaks

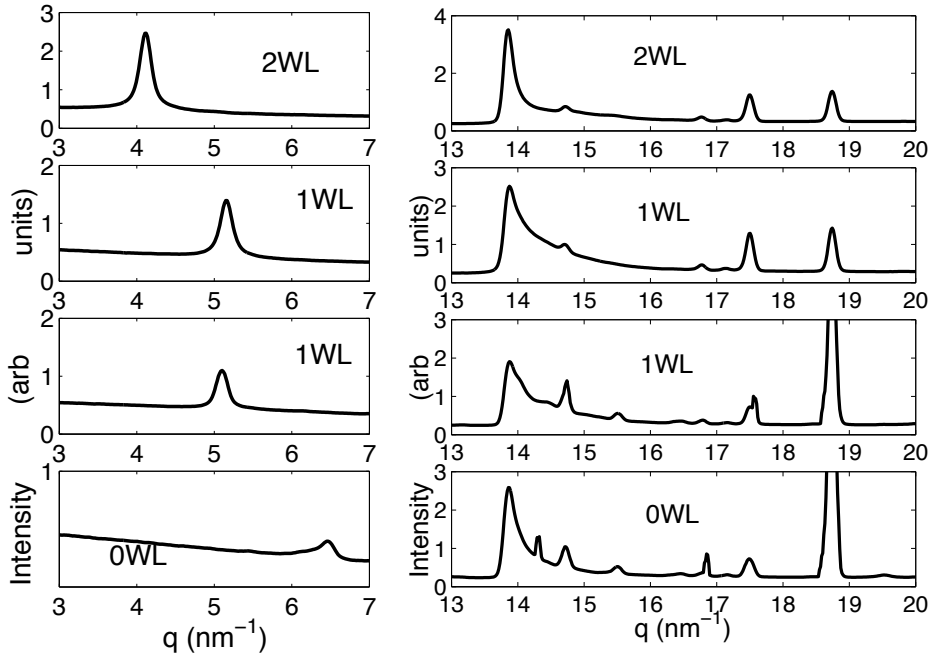

Figure 22: In-plane peaks for NaFLHC
Explanatioins in the text.
2wl, 1wl up : NaFLHC Lutnaes-1 ; 1wl down, 0wl : NaFLHC Lutnæs-2 sample

Hydration state	q001	q100	q101	q102
0WL	4.1	13.85	14.4	14.7
1WL	5.15	13.85	14.7	17.3
2WL	6.47	13.85	15.3	18.9

Table 6: Peaks with mixed Miller indices (q in nm^{-1})

4.5 Distances and mass loss

We can now compare the d001 distances obtained from X-ray data to the masses obtained from TGA data. Unfortunately, our data allow us to perform the comparison only for Na and Ni fluorohectorite, because some distances are missing for Li and Fe fluorohectorite. The mass of water absorbed is the difference of equilibrium masses at two distinct hydration states. Since the number of water molecule and their mass is linked by the mass of a single particle, which remains constant, we can write (using notations of section 2.1.3) :

$$\frac{n_2}{n_1} = \frac{m_{3\mathrm{WL}} - m_{2\mathrm{WL}}}{m_{2\mathrm{WL}} - m_{1\mathrm{WL}}}$$

The inequality(1) becomes :

$$\frac{m_{3\mathrm{WL}} - m_{2\mathrm{WL}}}{m_{2\mathrm{WL}} - m_{1\mathrm{WL}}} > \frac{d(2) - d(0)}{d(1) - d(0)} \tag{8}$$

In this table are shown these values for nickel and sodium fluorohectorite :

As we can see, the inequality is fulfilled for Na-fluorohectorite : Though, logically speaking, it cannot give us much more informations, it should at least indicate that Na-fluorohectorite does not shows strange behavior and that each of the hydration transition

Table 7: Relative mass gain and relative d-spacing gain during transition.

Sample	$\frac{n_2}{n_1}$	$\frac{d(2)-d(0)}{d(1)-d(0)}$
Na	3.28	2.26
Ni	1.31	1.55

may be analyzed as a first-order phasis transition. Ni-fluorohectorite, however, is not that easy to handle : of course, there could be a lot of reasons to explain the result opposite to what we expected. The one which is, I think, the most relevant is that, as explained before, in multi-valent cationic fluorohectorite (Ni, Fe...) the second water layer is not very clear : as said in section 4.1, because of different configurations possible in the interlayer space, the absorption of water molecules of the second layer is not a clear step at a given temperature. Or one of the hypothesis resulting to (1 was that hydration transitions were of the first order. Consequently we have to think that here things are more complex (several transitions ? not a first-order transition?) and that a single first-order transition is not a good model.

Conclusion

Conclusion for experiments The improvements brought on experimental set-ups seem to work well. Program made with Labview to control temperature gave satisfactory results throughout experiments, and simplified our task to relate temperature to X-ray spectrum. In the same time, we were in TGA experiments able to cool down to 0°C, which had not been done the previous years. Concerning TGA data, the main results are equilibrium masses for lithium and iron fluorohectrite (from which we deduce transition temperatures), never measured before, as well as an evidence of the absorbency of 3 water layers for Fe-fluorohectorite. Meanwhile, X-ray data provided some interlayer distances never measured for lithium and iron fluorohectorite ; they also showed that for iron, some shifts in pure state peaks could occurs, like for Ni, due to rearrangement of interlayer water spatial configuration, perturbing the measurement of the concerned pure state. However, these data did not show any displacement of in-plane peaks during hydration transition, as expected though.

Further work suggested It could be great to perform other TGA experiments with a better Temperature resolution (1°C) to get more precise transition temperatures, and both in cooling and heating to study hysteresis. Concerning X-ray study, since the pure-state characterization requires longer time than what we had in ESRF, it would be better to perform it with samples maintained for a long time in given Temperature and Humidity environment (for example in NTNU x-ray laboratory). In addition, since similar samples did not provided exactly the same spectra, it could be interesting to study aging in these samples, specially with parameters like sample size and shape. Moreover, additional studies of in-plane peaks are definitely required in order to be sure that these peaks are moving (or not), a problem still not resolved.

References

[1] T.N. Aalerud. Synchrotron x-ray scattering studies of water intercalation in synthetic nickel-fluorohectorite. Master's thesis, NTNU, Inst. for Fysikk, 2001.

[2] J. Als-Nielsen and D. McMorrow. *Elements of Modern X-ray Physics*, volume 1. Oxford University Press, New-York, 1997.

[3] D.L. Bish and C.J. Duffy. *Thermal analysis in Clay Science.* The Clay Mineral Society, 1990.

[4] G.W. Brindley and G. Brown. *Crystal structures of clay minerals and their x-ray identification.* Mineralogical society, 1980.

[5] C. Coussa. Raport de stage. Technical report, NTNU Inst. for Fysikk and Univ Paris-sud 11, 2003.

[6] G. J. da Silva, J. O. Fossum, E. Di Masi, and K.J. Måloy. Hydration transitions in a nanolayered synthetic silicate: A synchrotron x-ray scattering study. *Physical Review B*, 67, march 2003.

[7] G. J. da Silva, J. O. Fossum, and E DiMasi. Synchrotron x-ray scattering studies of water intercalation in a layered synthetic silicate. *Physical Review E*, 66, july 2002.

[8] L.W. Finger. *Modern Powder Diffraction*, volume 20. edited by D.L. Bish and J.E. Prost, 1989.

[9] Magnus Haakestad. Initial small-angle neutron scattering studies of synthetic clay sodium fluorohectorite. Master's thesis, NTNU, Inst. for Fysikk, jan 2001.

[10] S.B. Lutnaes. Experimental studies of water intercalation in a layered silicate system. Master's thesis, NTNU, Inst. for Fysikk, Feb 1999.

[11] D.M. Moore and R.C. Reynolds, Jr. *X-Ray diffraction and the identification and analysis of Clay Minerals*, volume 2. Oxford University Press, New-York, 1997.

[12] J. O. Mheust, Y.and Fossum, G. J. da Silva, K. D. Knudsen, G. Helgesen, and K.J. Mly. Hendricks-teller analysis of the intercalation transition in a fluorohectorite clay. preprint.

[13] N.T. Skipper, K. Refson, and J.D.C. McConnell. Computer simulation of interlayer water in 2:1 clays. *J.Chem.Phys.*, 94(11), june 1991.

[14] M. Suzuki, N. Wada, D. R. Hines, and M. S Whittingham. Hydration states and phase transitions in vermiculite intercalation compounds. *Physical Review B*, 36(5), august 1987.

[15] N. Wada, D. R. Hines, and S. P. Ahrenkiel. X-ray-diffraction studies of hydration transitions in Na vermiculite. *Phys. Rev. B*, 41(18):12895–12901, 1990.

[16] G.K. Werthem, M.A. Butler, K.W. West, and D.N.E. Buchanan. *Rev. Sci. Instrum.*, 45, 1974.

[17] G.K. Williamson and W.H. Hall. X-ray line broadening from filed aluminium and wolfram. *Acta Metallurgica*, 1, jan 1953.

List of Figures

5 Appendix

A Fits results for X-ray data

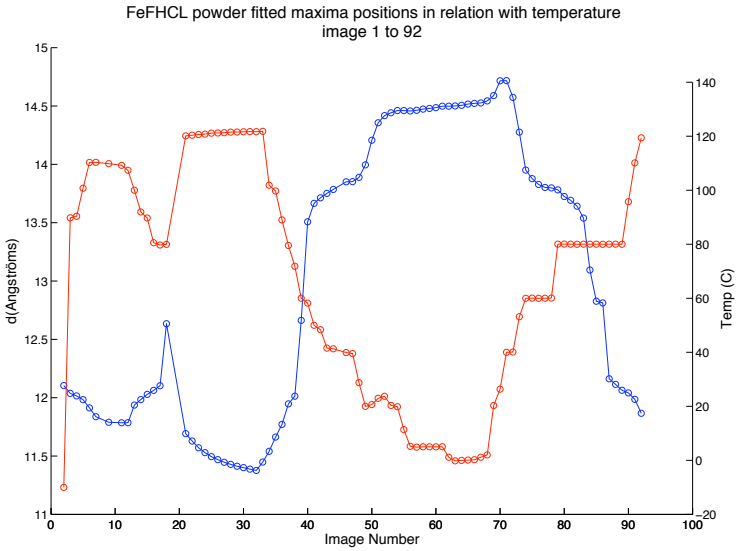

Figure 23: FeFLHC fitted d001(blue) and temperature (red) vs time

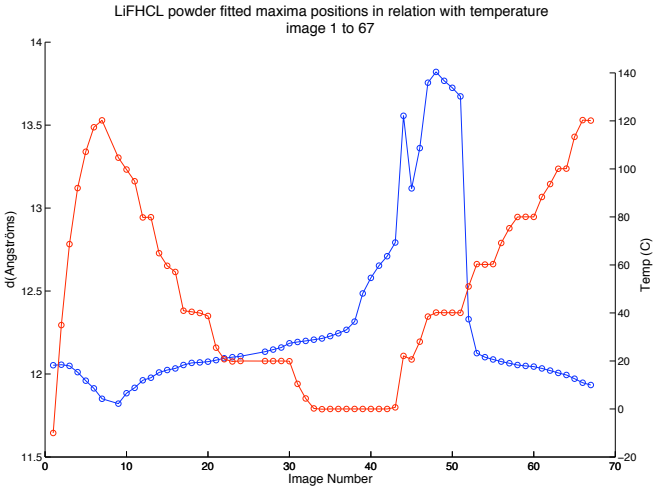

Figure 24: LiFLHC fitted d001(blue) and temperature (red) vs time

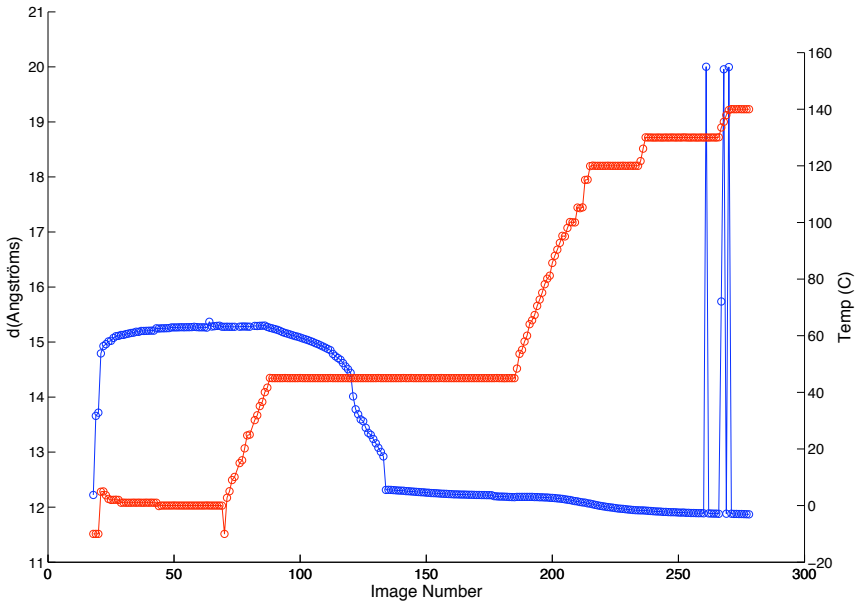

Figure 25: Na Lutnæs-1 fitted d001(blue) and temperature (red) vs time

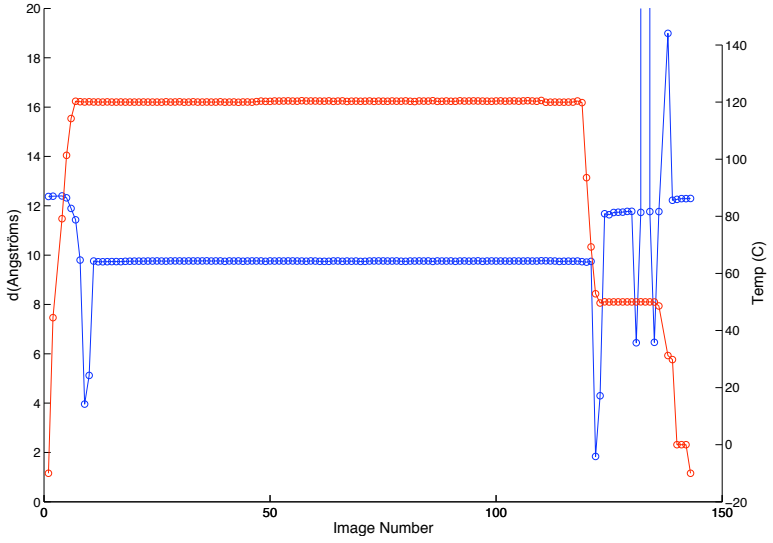

Figure 26: Na Lutnæs-2 fitted d001(blue) and temperature (red) vs time

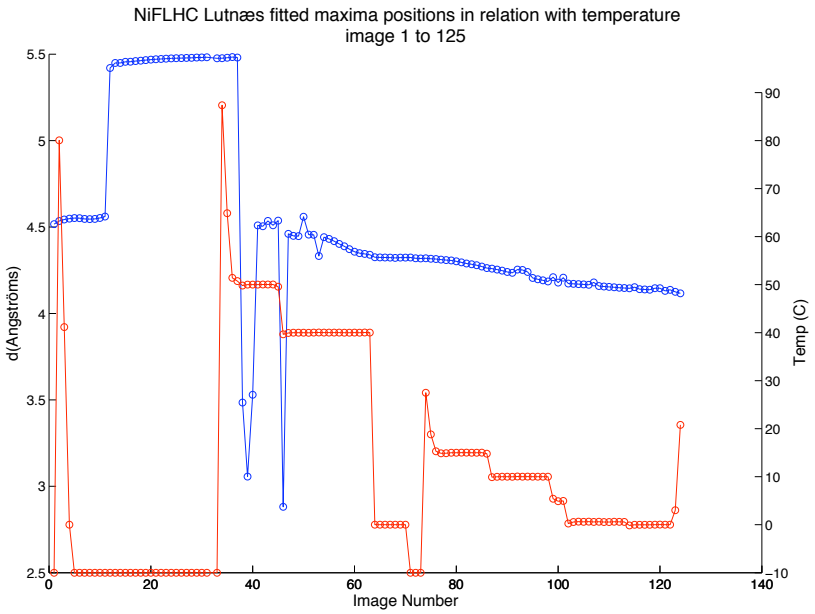

Figure 27: Ni Lutnæs fitted d001(blue) and temperature (red) vs time

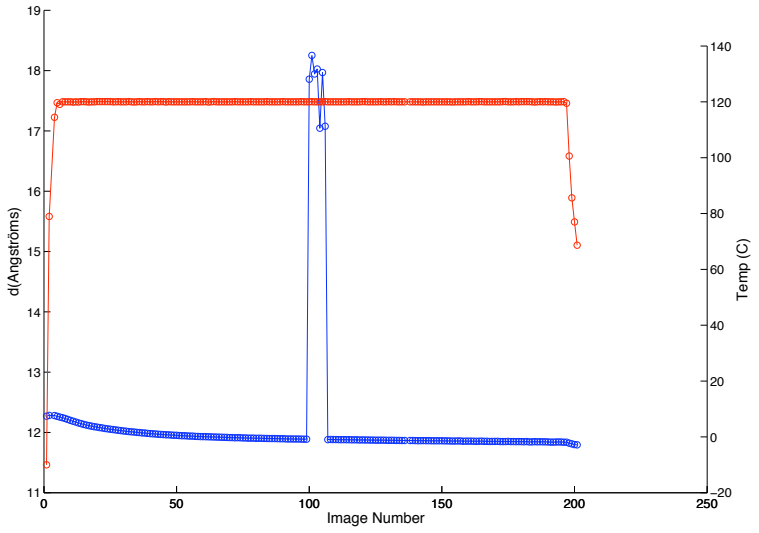

Figure 28: Na 10t fitted d001(blue) and temperature (red) vs time

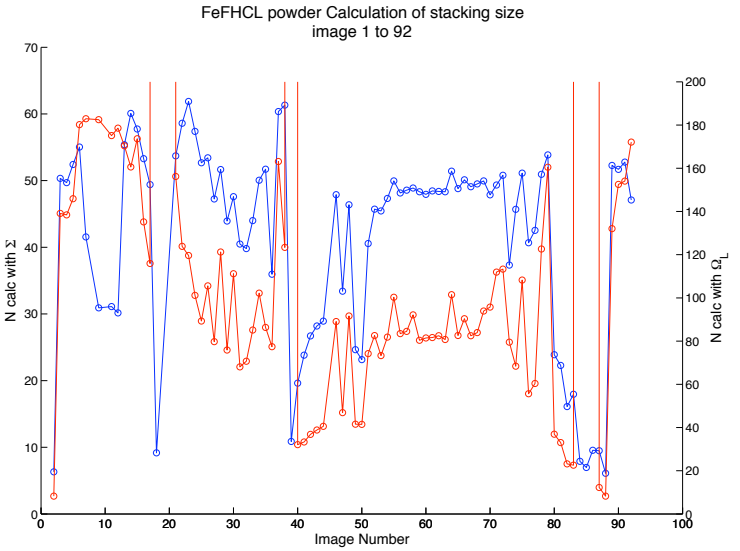

Figure 29: FeFLHC Stacking size calculated with Γ (blue) and Ω_L (red)

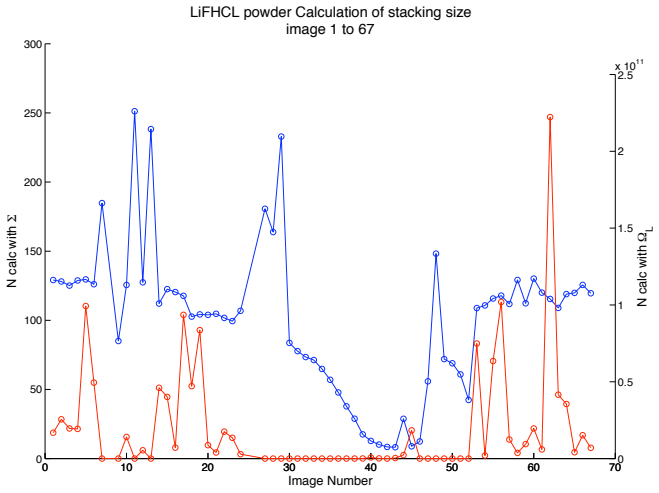

Figure 30: LiFLHC stacking size calculated with Γ (blue) and Ω_L (red)

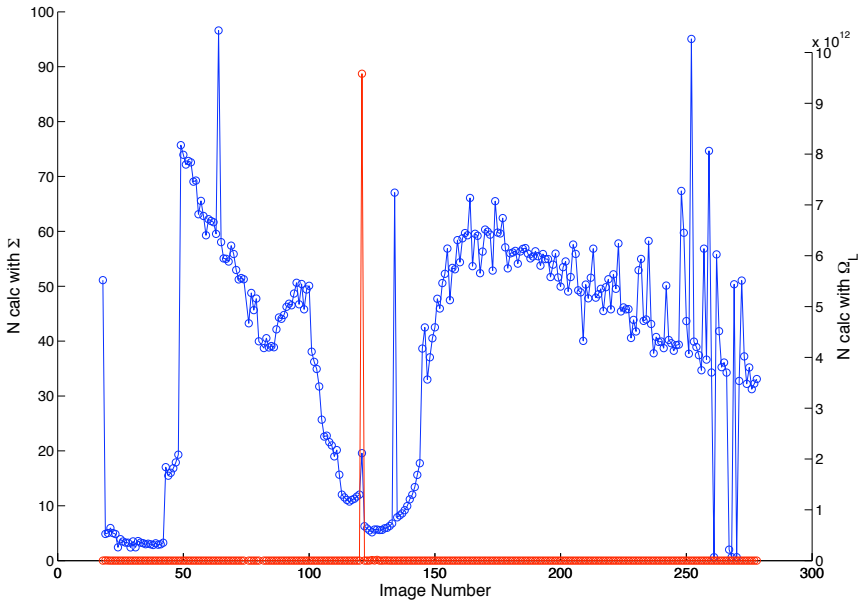

Figure 31: Na Lutnæs-1 stacking size calculated with Γ (blue) and Ω_L (red)

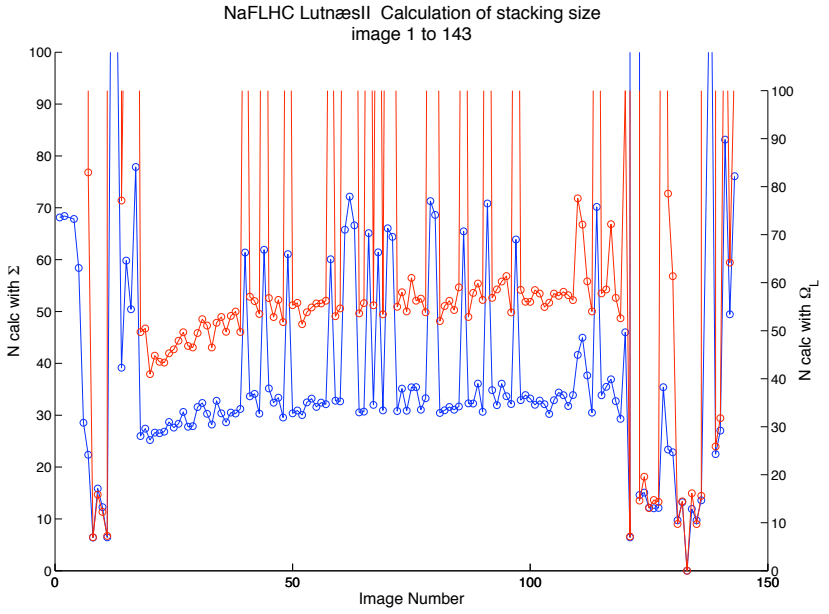

Figure 32: Na Lutnæs-2 Stacking size calculated with Γ (blue) and Ω_L (red)

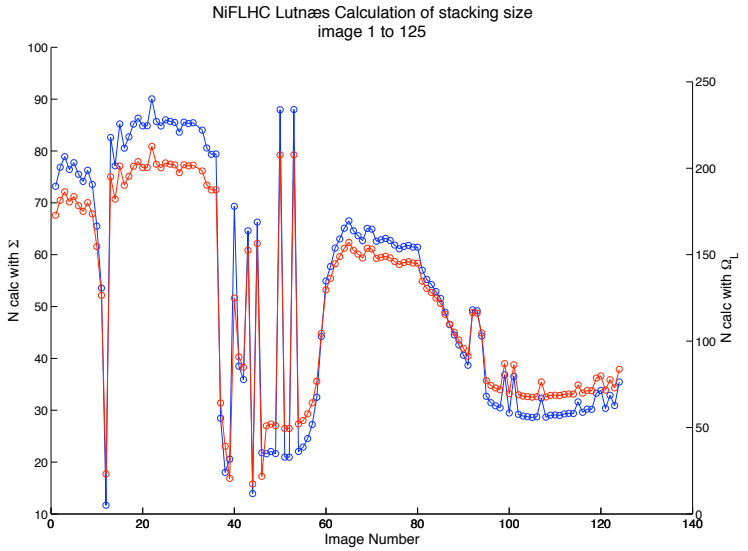

Figure 33: Ni Lutnæs stacking size calculated with Γ (blue) and Ω_L (red)

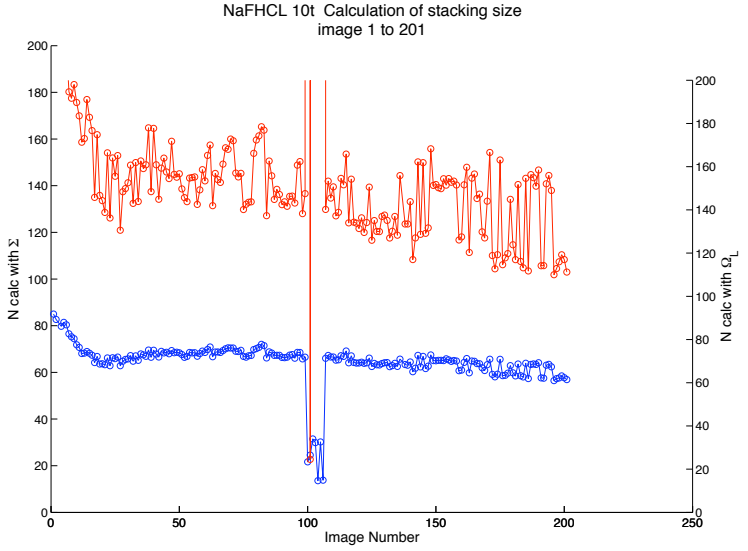

Figure 34: Na 10t stacking size calculated with Γ (blue) and Ω_L (red)

B Labview program

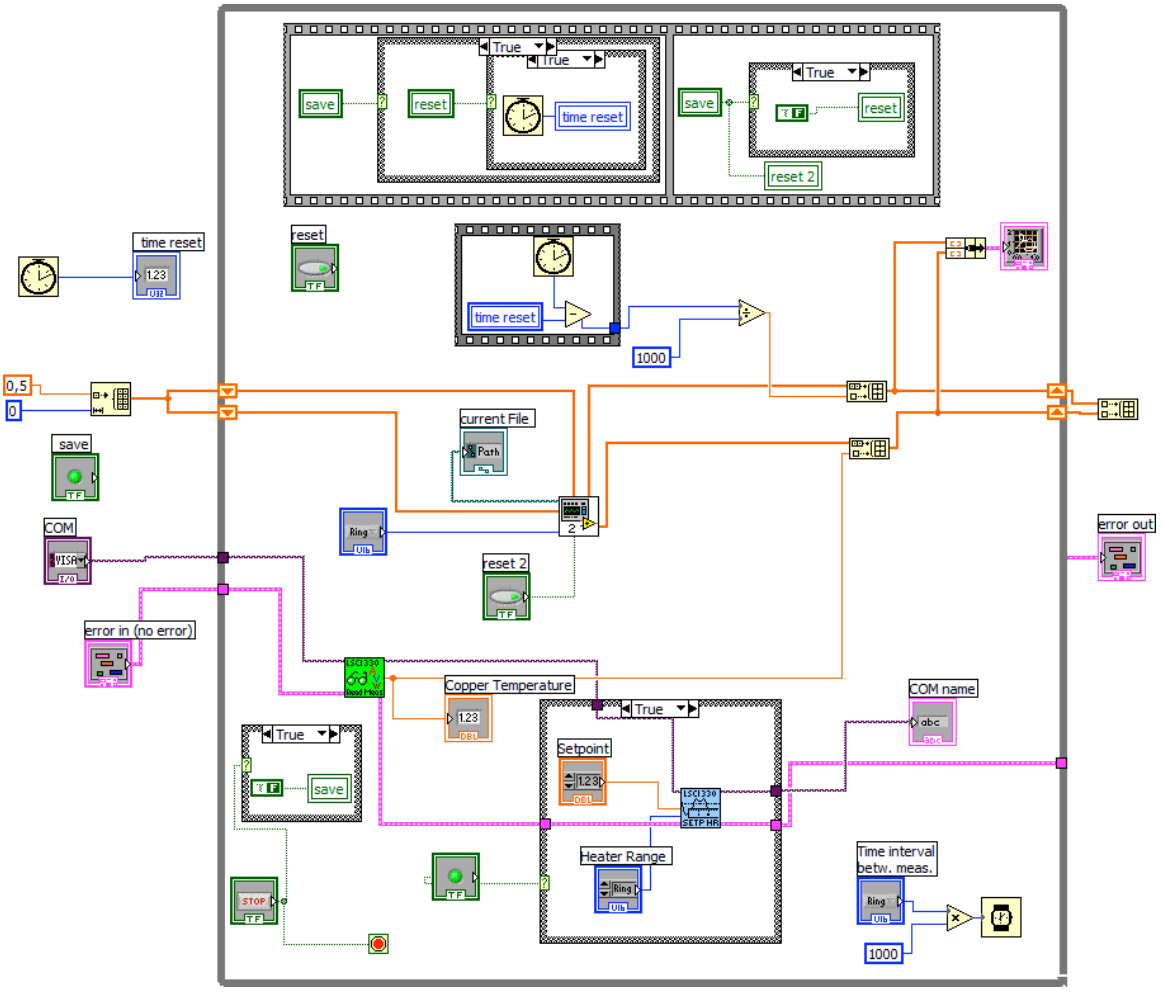

Figure 35: temperature control labview program

C Rocking scans

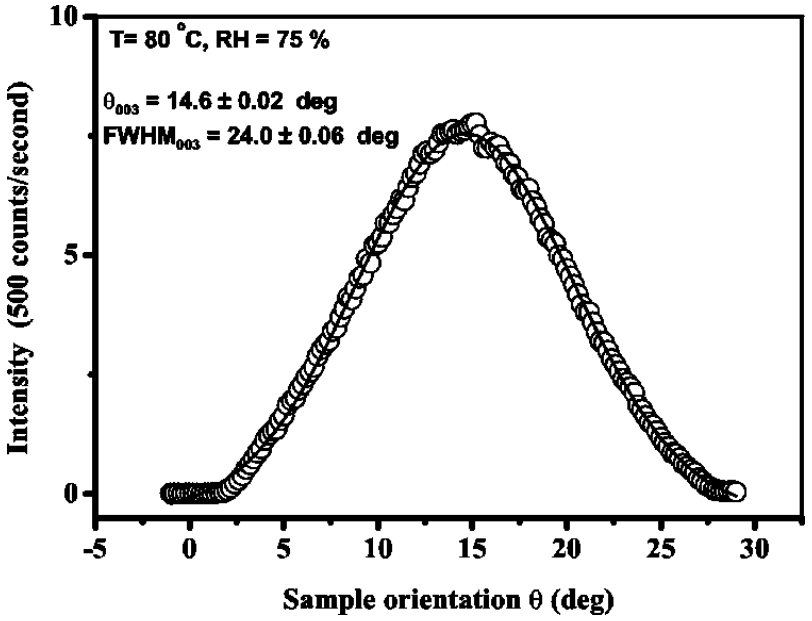

Figure 36: Lutnaes sample Rocking scan

D TGA derivative samples

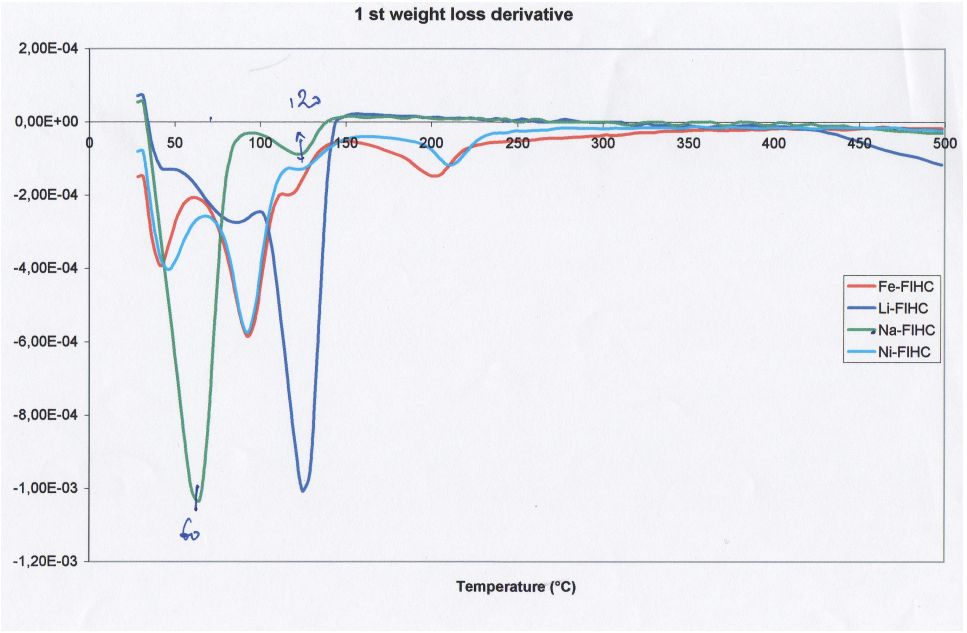

Figure 37: TGA derivative curves (courtesy of Ahmed Gmira)
the derivative curves show transition temperatures at peak maxima. However, since the heating rate is large (10°c s^{-1}), the transformation is not quasistatic and then there is a shift in the temperatures values.

E Example of Mar345 picture

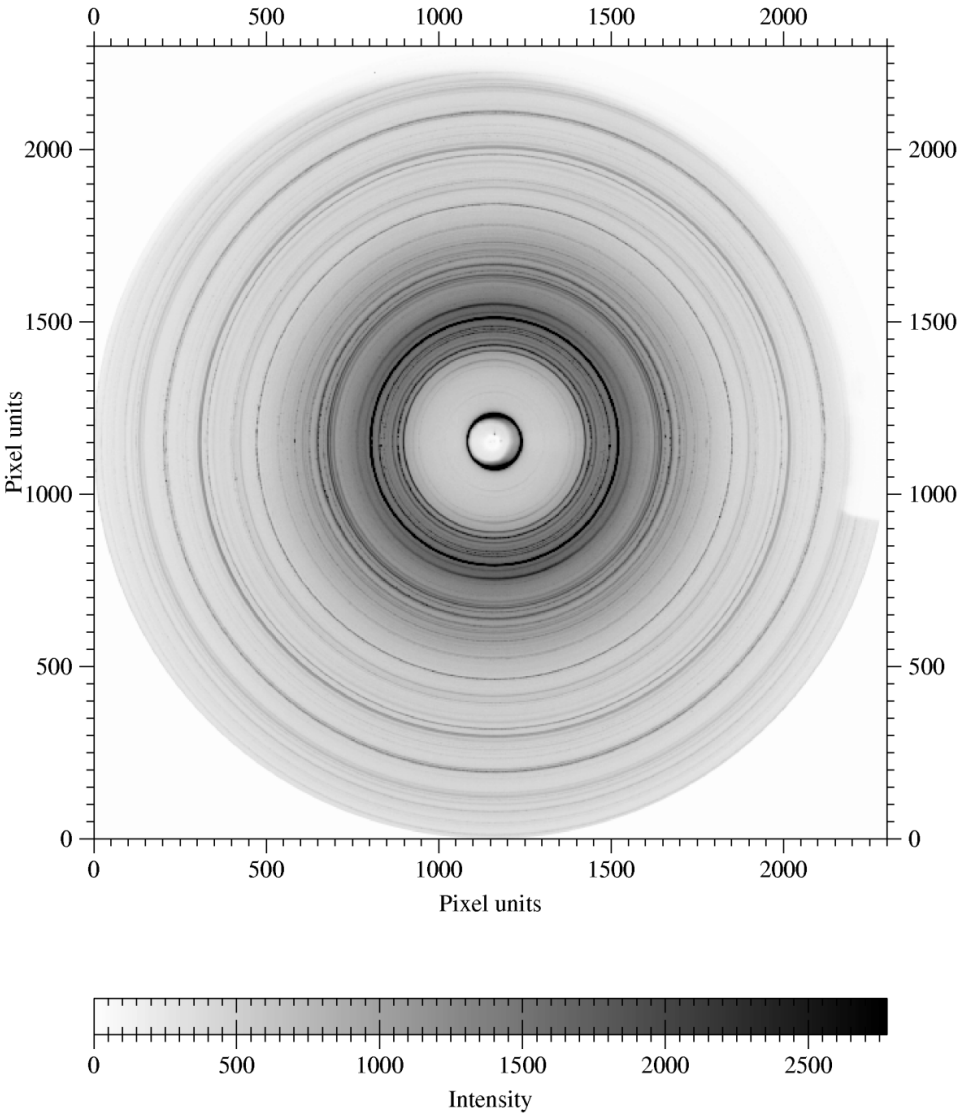

Figure 38: Example of Mar345 picture.
black levels correspond to intense levels. Fit2D software is able to perform a circular integration on these kind of picture, and the result is a spectrum like fig.17.